UNIVERSITY OF CALIFORNIA
RIVERSIDE

Glacial Chronology of a High Altitude Moraine Series, Tamarack Bench/Francis Canyon, Sierra Nevada, California

A Thesis submitted in partial satisfaction
of the requirements for the degree of

Master of Science

in

Geological Sciences

by

Daryl Lee Kohut

August 2011

Thesis Committee:

Dr. Richard Minnich, Chairperson
Dr. Mary Droser
Dr. Martin Kennedy

The Thesis of Daryl Lee Kohut is approved:

_____

_____

_____

Committee Chairperson

University of California, Riverside

ACKNOWLEDGMENTS

I would first and foremost like to thank Dr. Martin J. Kennedy for instituting the Global Climate and Environmental Change program at the University of California Riverside, for taking me on as a student, and for his guidance and support. Without him and his program I would not have had this amazing experience. I would also like to thank my advisor Dr. Richard A. Minnich for all his guidance in writing and his vast knowledge of atmospheric physics, and committee member Dr. Mary L. Droser for her tireless assistance with all things outside the classroom. A special thank you goes to Dr. Lewis Owen and everyone in his lab at the University of Cincinnati for going above and beyond what was asked of them in assisting me. My good friends and colleagues Michael Trumbower and Baird King provided an infinite reservoir of energy and assistance during an epic summer of fieldwork without whom this project would not have been completed. Others whose support was invaluable to my work include: Tiffany Wisser, Shirley Kohut, Kurt Kohut, Dr. Peter M. Sadler, members of the Global Climate and Environmental Change lab, the Earth Science Department at the University of California, Riverside, Earth Science Department at the University of Cincinnati, Sierra Nevada Aquatics Research Laboratory, everyone at White Mountain Research Center, Margie DeRose, and United States Forest Service. For inspiration I would like to thank Dr. Sarah Tindall and everyone in the Department of Physical Sciences at Kutztown University. Financial support for this thesis from: Sierra Nevada Aquatic Research Lab, and the National Science Foundation.

DEDICATION

“If I have seen further it is by standing on the shoulders of giants.”

-Isaac Newton

This thesis is dedicated to my family for letting me stand on their shoulders, and providing me with unwavering support for any and all endeavors I have ever pursued, and to Tiffany for setting me on this path all those years ago.

ABSTRACT OF THE THESIS

Glacial Chronology of a High Altitude Moraine Series,
Tamarack Bench/Francis Canyon, Sierra Nevada, California

by

Daryl Lee Kohut

Master of Science, Graduate Program in Geological Sciences
University of California, Riverside, August 2011
Dr. Richard Minnich, Chairperson

Alpine glaciers in the Sierra Nevada are sensitive to regional climate fluctuations and preserve a high resolution record of climate change in the form of glacial deposits (surficial and lacustrine). Fluctuations of alpine glaciers signify shifts in precipitation and temperature. Developing a regional chronology of changes will enable correlation to regional and global climate records, assist in understanding the mechanisms behind these shifts, and help predict possible future changes. A chronology of a high altitude moraine series on the Tamarack Bench /Francis Canyon, eastern Sierra Nevada showing a complex late Pleistocene retreat during MIS 2 was developed through mapping and dating of 3 glacial deposits: TBm2 (18.8 ka), FLm2 (16.6 ka), and FCm3 (12.6 ka) using terrestrial cosmogenic nuclide ^{10}Be. Currently no standard practice exists for

interpretation of cosmogenic nuclide ages creating problems with correlation. Here I present a method of interpretation through application to our data and critical evaluation of current regional studies. Attempts at resolving the timing of the regional Recess Peak advance in the Sierra Nevada using only TCNs will be unsuccessful until accuracy improves.

Table of Contents

List of Figures

Introduction

Methods

Results

Discussion

List of Tables

Introduction

The study of past climate change is important to understand how our climate system works so society can anticipate future changes, particularly the delivery of precipitation. To predict these changes we must understand the mechanisms behind climate shifts, which will require regional and global correlation of past climates using proxies preserved in the geologic record.

The Sierra Nevada (SN) records a regional climate signal and its variance through time in lake sedimentation and glacial deposition. The SN is the first orographic barrier to Pacific Ocean moisture transported seasonally onshore in California by the jet stream. During winter, the jet stream migrates south due to an increased latitudinal temperature gradient caused by change in insolation due to Earth's orbit (Minnich, 2007). Orographic uplift and cooler temperatures cause the majority of precipitation to fall in the form of snow (Owen *et al.*, 2003). Lake sedimentation and glacial deposition record changes in this signal. This record is one of the most well preserved in the United States due to the arid climate of the eastern SN (Phillips *et al.*, 1990).

The glaciers which exist currently in the SN are products of this climate pattern. Today glaciers are small and confined to their cirques. The presence of the more extensive moraines is a testament to the previous existence of larger glaciers, and the change in climate that caused their retreat and disappearance.

There have been many studies on the SN glaciation, but few have focused on the less extensive, younger, higher elevation moraines (Clark and Gillespie, 1997). Currently

the climate record preserved in lake sediments in the SN suggests that the high elevation morphological evidence is incomplete (Konrad and Clark, 1998). Since alpine glaciers are sensitive to small climate fluctuations, finding a more complete morphologic record and correlating it with the sedimentary record would provide a more detailed picture of how climate varied in the eastern SN.

Attempts at dating the morphologic record of SN advances come from ^{36}Cl cosmogenic nuclide ages (Phillips *et al.*, 2009; Phillips *et al.*, 1996; Phillips *et al.*, 1990). These studies focus on moraines at significantly lower elevations rather than the moraines in or near the cirques. Chlorine 36 production rates have an external uncertainty of 10% to 15% which is not addressed in these studies (Phillips *et al.*, 2009) (Table 1, pg 3) because all samples within the same study area will be affected equally by external uncertainties. When comparing results from different nuclides, regions, or to independent age records external uncertainties need to be considered. Since the uncertainty in production rates translates directly into uncertainty of the exposure age, the ages cannot be known more accurately than the production rates (Dunai, 2010).

TCN dating has led to uncertainty in correlating SN glacial advances to the Younger Dryas cold event at 12.5 ka. Age calculation in this time frame creates an error of ~1 ka which is approximately equivalent to the duration of the Younger Dryas event.

A standard procedure for interpreting cosmogenic ages remains elusive. The age resulting from TCN dating shows how long that particular surface has been exposed to incoming cosmogenic radiation, because the accumulation of TCN in rock surface is a

Table 1 Sources of uncertainty.		
Analytical/Observational (2-6%)	Internal Uncertainty	
Sample parameters (<1-5%)		Random
Elevation Surface geometry (self-shielding)		Random
Sample thickness		Random
Thickness and density of overburden (soil, rock)		Random
Preparation (1-3%)		
Cross-contamination		Random/systematic
Sample weighing		Random
Carrier weighing		Random
Dilution of target mineral by non-target minerals		Random/systematic
Stable isotope measurement (e.g. 27Al for 26Al)		Random
Target element chemistry		Random
Major and trace elements (for neutron flux calculations, 36Cl; 3He)		Random
AMS or NG-MS (1-5%)		
Counting statistics (standards and samples)		Random
Machine background correction		Random
Blank correction		Random
Correction for non-cosmogenic components		Random
Characterization of standard material		Random/systematic
Methodological (5-15%)	External Uncertatinty	
Radionuclide half-life		Random/systematic
SLHL-production rate		Random/systematic
Cosmic ray flux attenuation in rocks		Random/systematic
Scaling factors		Random/systematic
Angular dependency of cosmic ray flux in the atmosphere		Random/systematic
Secular variation of atmospheric pressure, magnetic field, solar modulation		Random/systematic
Geological/natural (0-100%)		
Assumed erosion rate and style (for age correction)		Systematic
Shielding correction (snow, vegetation etc.)		Systematic/random
Pre-exposure		Random
Exhumation		Random
Misjudgment of the geomorphologic context of a surface		Sytematic

Table 1 Modified from Dunai, 2010

function of time. The age of moraines is assumed to represent the process of glacial entrainment and transport that removes previously accumulated isotopes through abrasion. Moraine clasts each have unique transport and exposure histories. Outliers of a data set are excluded based on statistical analysis, reflecting exposure inheritance, loss of material due to fire spalling, or lowered accumulation from exhumation post deposition. The remaining ages overlapping within ±2σ uncertainty can be used to represent the age of the geological feature. Other practitioners consider all data, i.e. no

outliers are removed (Dunai, 2010). In some instances the age of the feature is represented by a single boulder considered to be the best sample based on field assessment. These varying analytical approaches change the significance of mean ages of sampled boulders and inhibit correlations between studies and regions.

The Recess Peak is considered to be the last Pleistocene advance in the SN. The best age constraint for its timing is 13.1 ±.09 ka (Clark and Gillespie, 1997) based on a ^{14}C date of organic silt at the gyttja/outwash transition in a Baboon Lakes core inside the inner most Recess Peak recessional moraine in Bishop Creek drainage. A ^{14}C age from gyttja at the gyttja/outwash transition in the central Baboon Lake yielded an age of 12.8-12.7 ka (Clark and Gillespie, 1997). Four ^{36}Cl ages obtained from the Recess Peak terminal moraine at Baboon Lakes yielded an average of 12.5 ±4.4 ka (Phillips *et al.*, 2009). However, based on field assessment the best sample was considered to be from a terminal moraine in the South Fork of Bishop Creek at Treasure Lakes (13.3 ±0.6 ka) (Phillips *et al.*, 2009) and was considered representative of the advance. Since error only incorporates the analytical uncertainty in the ^{36}Cl measurement, a possible Younger Dryas age cannot be ruled out.

Other records for the late Pleistocene/Holocene transition are conflicting. Surficial record suggests 4 advances in the last 30 ka (Phillips *et al.*, 2009). The Owens Lake record suggests an incomplete record from Bishop Creek showing 19 SN glaciations occurring from 55 to 11 ka (Benson *et al.*, 1996). Open/closed regimes in Owens Lake occur in concert with GISP II from 155 to 60 ka and are in agreement with the Devils

Hole record (Li *et al.*, 2004). Dry events occur in concert with GISP II cold events (Benson *et al.*, 1998) across the Pleistocene/Holocene transition. The Owens Lake record of rock flour proxy data shows general agreement with the Atlantic marine record (DSDP 609) and Greenland (GISP II) from (79 - 15 ka) (Bischoff and Cummins, 2001) (Figure 1, pg. 6).

Data currently constraining the Pleistocene/Holocene transition in the SN show the region independent of the Atlantic climate and other North American alpine glacial records. Few studies have used cosmogenic isotope beryllium-10 to address glacial chronology in the SN (Nishiizumi *et al.*, 1989). Because ^{10}Be's production rate in quartz is relatively well constrained (~10% uncertainty), it is an ideal choice for use in the SN granodiorite. This study focused on a ^{10}Be TCN chronology of a complex series of high elevation (>3000 m) moraines deposited by alpine glaciers in Francis Lake Canyon and the Tamarack Bench (tributaries of Rock Creek) in the eastern SN (Figure 2, pg. 7). These moraines may correlate with an equally complicated glacial record evidenced in cores of Francis and Kenneth Lake located in Francis Canyon and the Tamarack Bench. Dates from these cores suggest possible ages of 8.2, 5.5 - 4.3, 1.6, and 0.6 ka (King, 2010; Trumbower, 2011). The chronology of glacial advances in Francis Canyon and the Tamarack Bench is used to address the problem of past complexity and variability in California's SN climate.

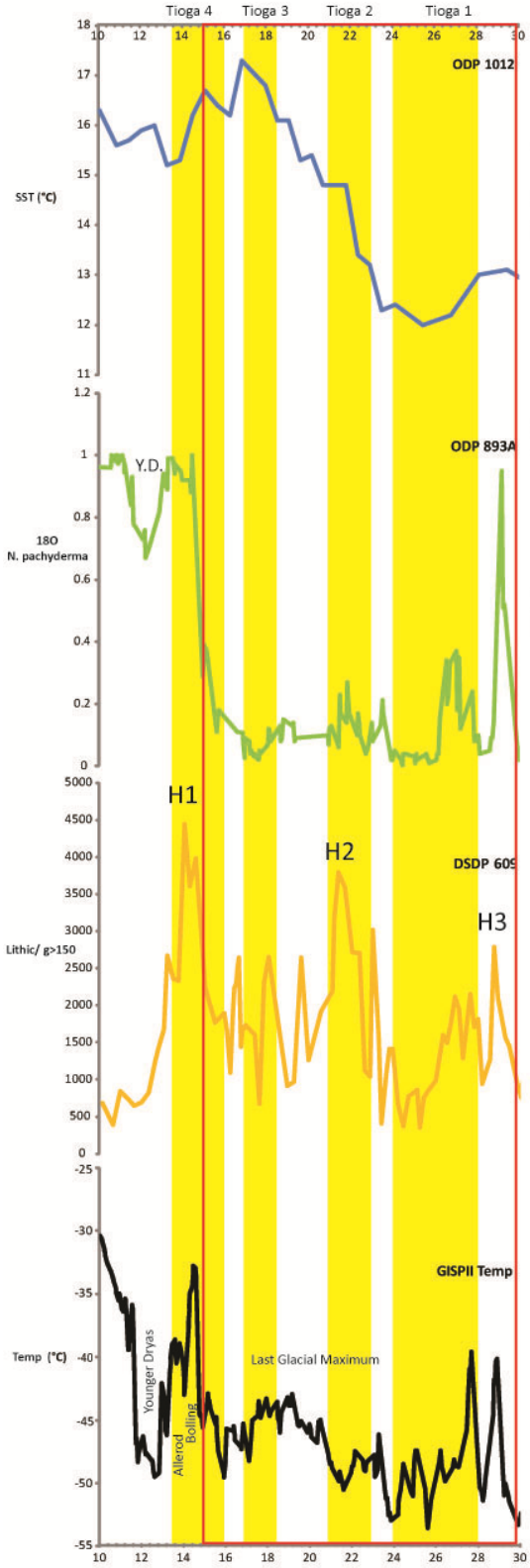

Figure 1: Correlation of global climate records with Sierran regional events. Timescale in ka. All data from WDC for Paleoclimatology online database.

ODP 1012 data originally from: Herbert et al., 2001.

ODP 893A data originally from: Hendy et al., 2007.
Santa Barbara Basin ODP893A Planktonic Stable Isotope Data
IGBP PAGES/World Data Center for Paleoclimatology
Data Contribution Series # 2007-080.
NOAA/NCDC Paleoclimatology Program, Boulder CO, USA.

DSDP 609 data originally from: Bond et al., 1992.

GISP 2 temperature data originally from: Alley, R.B.. 2004.
GISP2 Ice Core Temperature and Accumulation Data.
IGBP PAGES/World Data Center for Paleoclimatology
Data Contribution Series #2004-013.
NOAA/NGDC Paleoclimatology Program, Boulder CO, USA.

Cosmogenic ages for Tioga advances from: Phillips et al., 2009.

Red Box = S1 from: Bischoff and Cummins, 2001.

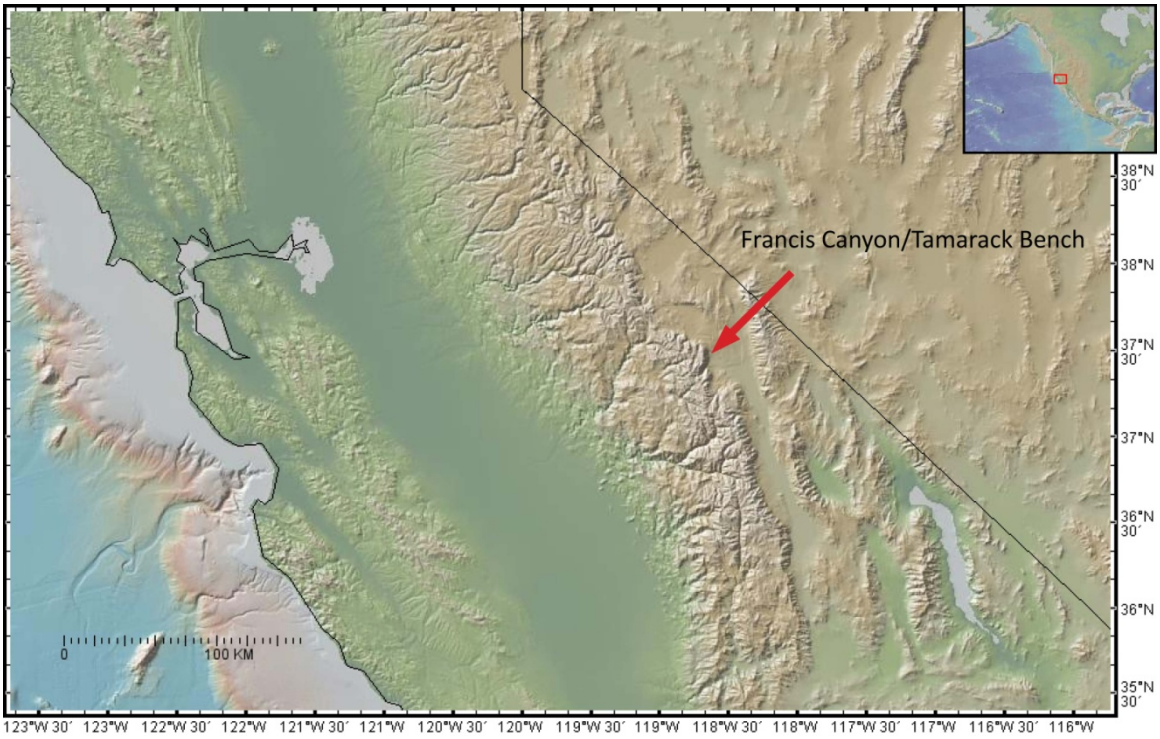

Figure 2: Study location map.

Critical evaluation of preexisting and new cosmogenic and lake core data allows for an alternative interpretation of late Pleistocene early Holocene glacial record. In this study I propose a standard procedure for interpretation of cosmogenic nuclide data.

Background

Setting and Regional Climate

Located in California, the SN is a north–south trending, west-tilted fault block uplifted by extensional basin-and-range faulting to the east. The SN separates the internally drained basins to the east from the Central Valley to the west and extends from the Tehachapi Mountains in the north to the Mojave Desert in the south.

Elevations along the crest range from 3400 to 4300 m. This range is a batholith of Mesozoic granodiorite intruded into metamorphic marine sedimentary and island-arc volcanic rock. The sedimentary and island-arc rocks exist as roof pendants (Gillespie and Zehfuss, 2004). Studies performed using stable isotope analysis to recreate paleo-elevations suggest uplift in the SN began in the late Cretaceous or early Cenozoic, and that modern faulting is the result of basin-and-range subsidence (Henry, 2009). Evidence of past climate change going back 2700 ka is well preserved (Huber, 1981).

The eastern SN climate is Mediterranean with winter precipitation and summer drought in relation to its geographical location and orientation in the mid latitudes (30° and 45°N), 320 km from the Pacific Ocean. In summer the jet stream lies near 50°N and convective precipitation is precluded by the cool California current. The SN is a 650 km long barrier 4270 m high oriented perpendicular to the jet stream. The majority of the precipitation falls onto the western slopes with a rainshadow along the eastern escarpment (Powell and Klieforth, 2000). During the winter, the polar jet stream migrates south and brings moisture from the Pacific Ocean to the SN. The result is seasonal precipitation on the eastern slope in the form of snow. The southward migration of the jet stream is due to increased latitudinal temperature gradient. Nearly all winter precipitation is snow above 2500 m (Owen *et al.*, 2003). The much larger volume of ice in Pleistocene glaciers was controlled by a southern shift in the jet stream caused by the Cordilleran and Laurentide ice sheets, increasing precipitation and reducing temperatures (Antevs, 1938).

Francis/Tamarack Drainages

Francis and Tamarack drainages are northeast facing, parallel tributaries of the Rock Creek drainage eastern SN (map Plate 1, pg. 81). These drainages meet on the Tamarack bench where the slope angles lower and merge with the main Rock Creek drainage to continue to the valley floor near Highway 395. Our study area is leeward of the SN crest which provides better preservation history than other sites currently studied. Francis Canyon has an average slope of ~15%, Tamarack Canyon ~14%, and the Tamarack Bench ~10%. Multiple glacial landforms are preserved in each canyon. A glacierete lies in the cirque of Francis Canyon. Both canyons have morainal landforms preserved in their cirques at approximately 3680 m. Tamarack Canyon has 2 headwalls and corresponding cirques, one facing northeast and the other north. Total drainage area is ~6.04 km^2. There is bare striated bedrock, 4 post-glacial lakes, and 2 roche moutonees preceding the confluence of the Tamarack Bench. Francis Canyon has 1 headwall facing northeast and several morainal landforms preserved throughout the canyon to the Tamarack Bench. There are moutonees in the lower reaches of the canyon on the northeast side of Francis Lake, one of 2 post-glacial lakes residing in the canyon with a total drainage area of ~6.31 km^2. Both drainages are rain shadowed by the crest of the SN to the west. Vegetation in the upper reaches of the canyons is sparse and limited to shrubs and extremely low lying trees down to about 3360 m where full size White Bark Pine (*Pinus albacaulus*) becomes prevalent.

History of SN Glacial Study

The glaciation of the SN has been studied since 1865 beginning with the state survey under the direction of J. D. Whitney. John Muir in 1872 first described the current existence of glaciers in the SN (Blackwelder, 1931). Israel Russell in 1885 mapped several existing glaciers high in their cirques for the U.S. Geological Survey near their largest, youngest moraine deposits (Russell, 1885). In 1898, H. W. Turner and F. L. Ransome were the first to define two distinct advances in the SN (Blackwelder, 1931). W. D. Johnson was the first to document and recognize 3 distinct advances based on field notes from the late 1880's he left behind from his work with Russell which subsequently have never been published (Blackwelder, 1931). In 1918 Knopf was the first to publish a map distinguishing these advances (Blackwelder, 1931). Antevs (1925) began speculation about the correlation between the SN glacial advances and the advances in the central plains region of the U.S. (Antevs, 1925). Blackwelder (1931) was the first to apply relative dating (RD) techniques to classify the glacial epochs into four stages based on local names Tioga, Tahoe, Sherwin, and McGee. The use of RD was expanded upon (Sharp and Birman, 1963; Birman,1964; Sharp, 1969a; Sharp, 1972; Burke and Birkeland, 1979). The expansion of the glacial sequence was suggested with the addition of the Tenaya between Tioga and Tahoe, and the Mono Basin between Tahoe and Sherwin (Sharp and Birman, 1963). The chronology of neoglacial advances

was originally proposed in Birman's (1964) study "Glaciation Across the Crest of the Sierra Nevada, California". Those advances are post-Tioga; Hilgard, Recess Peak, and the Matthes.

The Casa Diablo was proposed between Tahoe and Sherwin (Curry, 1969). Potassium argon dating put the first bounding ages in place for the SN glaciations in Coyote Flat, Owens River Gorge, and McGee Mountain (Dalrymple, 1963). As early as 1979 Burke and Birkeland were challenging the additions of the Tenaya and Mono Basin by reassessing relative dating techniques. Owens Lake core analysis using radiocarbon dating and stable isotope geochemistry has shown evidence of multiple glaciations in the SN and provided more accurate age constraints (Benson *et al.*, 1996; Benson *et al.*, 1998). Recent lake core studies applying radiocarbon dates to glacially deposited sediment challenge the current neoglacial sequence consisting of Recess Peak and Matthes suggesting a greater number of advances over the Holocene (King, 2010; Trumbower, 2011; Konrad and Clark, 1998). These techniques require specific relationships between glacial deposits and the materials being dated, or are based on conditions inferred to result from glaciation.

The newest advancement in the study of glacial chronology is terrestrial cosmogenic nuclide (TCN) dating which allows direct dating of glacial landforms (Nishiizumi *et al.,* 1989; Phillips *et al.*, 1990, 1996; Gosse and Phillips, 2001; Zech *et al.*,

2004; Dunai, 2010). Phillips *et al.'s* (2009) TCN study suggests a return to the classical sequencing proposed by Blackwelder (1931) with the exception of the neoglacial advances.

Methods

Mapping/ArcGIS

Francis Canyon mapping was performed on the ground using U.S. Geological Survey topographic, 7.5 minute, 1:24,000 scale quadrangles (1994b) and NAIP 2009 DOQQ aerial imagery. The map was then digitized using ArcMap 9.3 GIS software. The extent of the mapping was designed to encompass post-LGM glacial deposits and to be comparable to Birman's (1963) and King's (2010) map. Francis and Tamarck Lakes Canyons were mapped from the confluence of Tamarack Bench and Rock Creek to their cirque headwalls in the southwest, and was defined in the west by the northeast trending ridge separating Francis Lake Canyon and Rock Creek and Wheeler Ridge on the east. Units were separated by stratigraphic relationships, weathering characteristics, and relative dating results. A section of the map was selected to show sample locations (Figure 3, pg. 13).

A distinction was made between glacial moraines and rock glacier deposits. Rock glacier deposits were considered to be of debris covered ice origin. No distinction could be made as to whether they were periglacial (ice of permafrost origin) or glacial. Rock glacier deposits were classified based on their distinct morphology of low slope angle

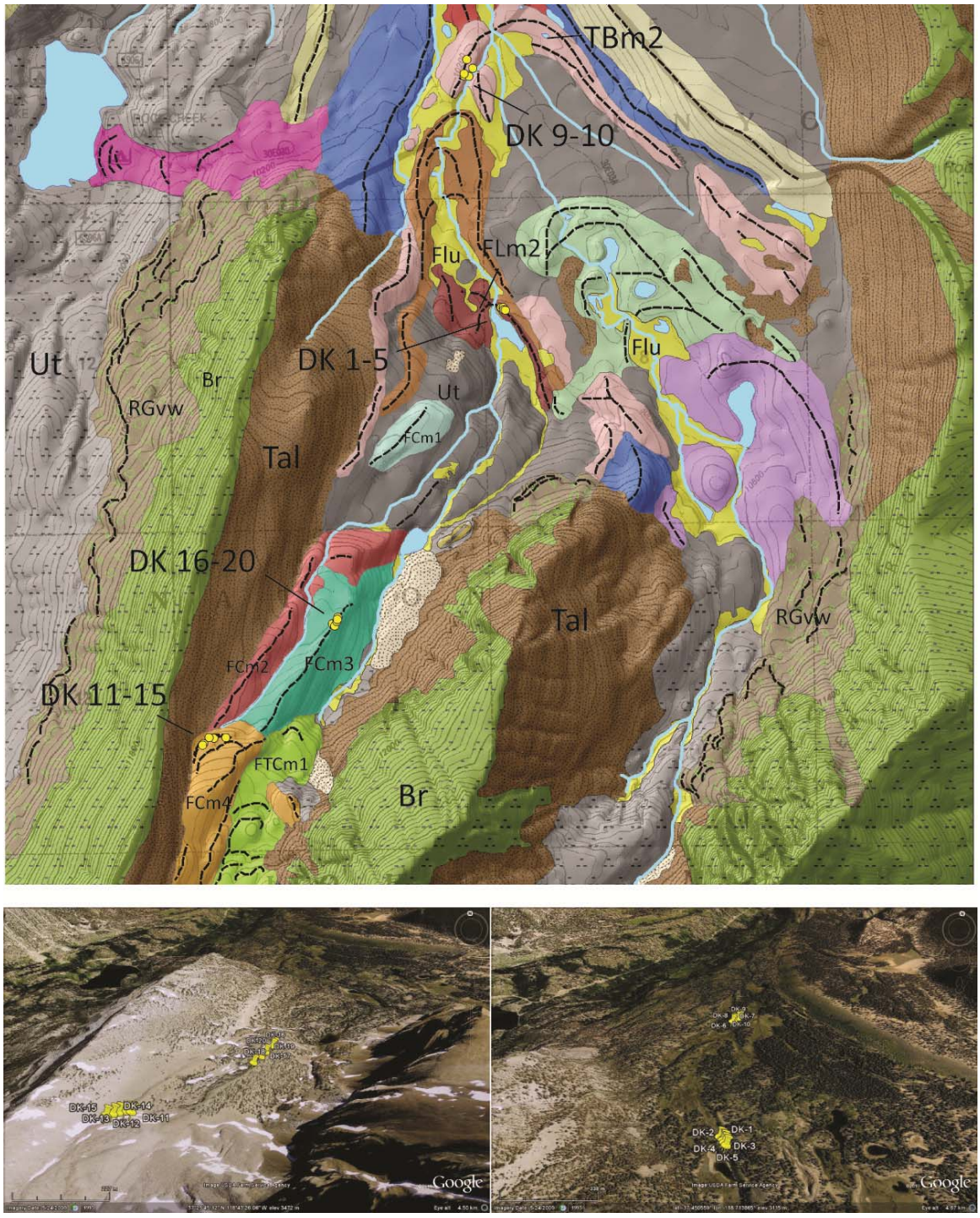

Figure 3: TCN sample locations.

benches extending from valley walls or cirque headwalls with lobate furrows in a continuous stream of talus and over steepened terminus slopes (Clark *et al.*, 1994; Konrad and Clark, 1998; Wahrhaftig and Cox, 1959). Glacial moraines were defined as unconsolidated, poorly sorted, sedimentary deposits located at previous ice margins resulting from the weathering and erosion processes of a glacier. There is no evidence that any rock glacier deposit was still active as no interstitial ice could be seen between boulders.

ArcMap

ArcMap 9.3 was used for digitizing. USGS, 15-minute digital elevation models (DEMs), 7.5-minute digital raster graphics (DRGs), and 5 meter U.S. Department of Agriculture (USDA) National Imagery Program (NAIP) digital ortho quarter quadrangles 2009 imagery were imported. A geo-data base was created for all images and data used. All maps and data were projected into California Teale Albers, North American Datum 1983 before analysis. Projections were performed using default settings.

Terrestrial Cosmogenic Nuclide Dating

Cosmic radiation was discovered in 1912 by physicist Victor Hess. Before the time of particle accelerators, cosmic rays were used as a source of high energy particles for studies of physics. It was not until A.V. Grosse in 1934 theorized that cosmic radiation could produce radioactive nuclides at the surface of the earth and that cosmic

radiation had potential applications to the earth science. In 1949 Willard Libby realized that ^{14}C was produced in measurable amounts at the earth's surface through interactions with the atmosphere (Gosse and Phillips, 2001). The method was originally applied only to lunar rocks and meteorites due to low terrestrial production rates. It was first applied to geology in 1955 by Raymond Davis and Oliver Schaeffer who measured ^{36}Cl in a mafic rock from the Rocky Mountains. In the mid-1980's, accelerator mass spectrometry allowed for precise measurement of the extremely low amounts of in situ terrestrial cosmogenic nuclide production in terrestrial rocks (Dunai, 2010).

The use of cosmogenic nuclide dating in Quaternary geology allows the direct dating of glacial landforms (Clark *et al.*, 1995), permitting the reconstruction of a high resolution record of regional glacial advance and retreat caused by climatic shifts (Gosse *et al.*, 1995; Owen *et al.*, 2003; Owen *et al.*, 2001). One of the first studies done in the SN was by Nishiizumi *et al.* in 1989.

The use of cosmogenics is increasing, and it is continuously being refined. Advances made in analytical methodology such as ^{36}Cl concentration determination, ^{36}Cl production rate calculation, and erosion rate calculation over the last 5 to 10 years are increasing the reliability of the most recent cosmogenic studies (Phillips *et al.*, 2009). Clark *et al.* (1995.) showed that geomagnetic strength varied over the Pleistocene and would also affect production calculations significantly. Several parameters need to be better understood to more accurately and precisely date short lived climatic events such as the Younger Dryas. These parameters are: long term-geomagnetic latitude of a

specific site, altitude and latitude scaling corrections, and muon contribution to ^{10}Be production (Clark *et al.*, 1995). New developments since the Clark *et al.* (Clark *et al.*) study are the muon contribution to TCN production, non-dipole components of the geomagnetic field, and the temporal and spatial variations in the paleo-atmosphere and surface elevation (Dunai, 2010; Gosse and Phillips, 2001).

TCN dating is based on the idea that the amount of a target nuclide in the surface being dated is the result of the cosmic ray bombardment over time due to exposure to the sky. If the TCN production rate is known, the resulting date can be calculated from the amount of the target nuclide present. Cosmic rays are high-energy charged, particles entering Earth's atmosphere from all directions. These high-energy charged particles originate in the Milky Way galaxy from supernovas occurring approximately once every 50 years. Charged particles include atomic nuclei, electrons, positrons, and other subatomic particles (Dunai, 2010). This particle bombardment is also referred to as galactic cosmic radiation (GCR) (Gosse and Phillips, 2001). There are two main types of cosmic rays, primary and secondary. Primary cosmic rays are composed mostly of protons (87%), α-particles (12%), and heavier nuclei (1%). These particles enter Earth's atmosphere and collide with atoms in the air. The energy of primary cosmic particles exceeds the energy which binds nuclei. The collisions subsequently result in spallation reactions. Spalled off nucleons from the target nucleus maintain the direction of the impacting particle (Dorman *et al.*, 1999). These spalled nucleons impact and produce other spallation reactions, causing a nuclear cascade in

the Earth's atmosphere, and secondary cosmic rays (Figure 4, pg. 18). Because protons suffer ionization losses with atmospheric depth (Lal and Peters, 1967), the dominant composition of the rays changes from proton to neutron. The resulting composition at sea level is 98% neutrons (Masarik and Beer, 1999).

Spallation reactions at Earth's surface produce TCNs or cosmic nuclides. Nuclides are atoms of an element with a unique number of protons and neutrons. A terrestrial cosmogenic nuclide is a nuclide produced by spallation reactions with atoms at Earth's surface in situ caused by secondary cosmic radiation (Dunai, 2010; Gosse and Phillips, 2001). ^{10}Be can be produced by reactions other than those through spallation in the target mineral such as: atmospheric spallation and muon interaction. ^{10}Be is also produced in the atmosphere through spallation with nitrogen and oxygen, and is deposited on the earth's surface. Atmospheric ^{10}Be also will penetrate dense rocks and adsorb to the surface of mineral grains and is 10^3 times greater than the cosmogenic ^{10}Be production in rock. Atmospheric contamination is dealt with during sample preparation through etching which removes ~30% of the target mineral (Dunai, 2010; Gosse and Phillips, 2001).

Muons are subatomic, have masses intermediate between protons and neutrinos, and are considered the heavier brother of the electron. These elementary particles have the ability to produce cosmogenic nuclides of ^{10}Be. Muons are created high in the atmosphere through collisions of primary cosmic rays with atomic nuclei

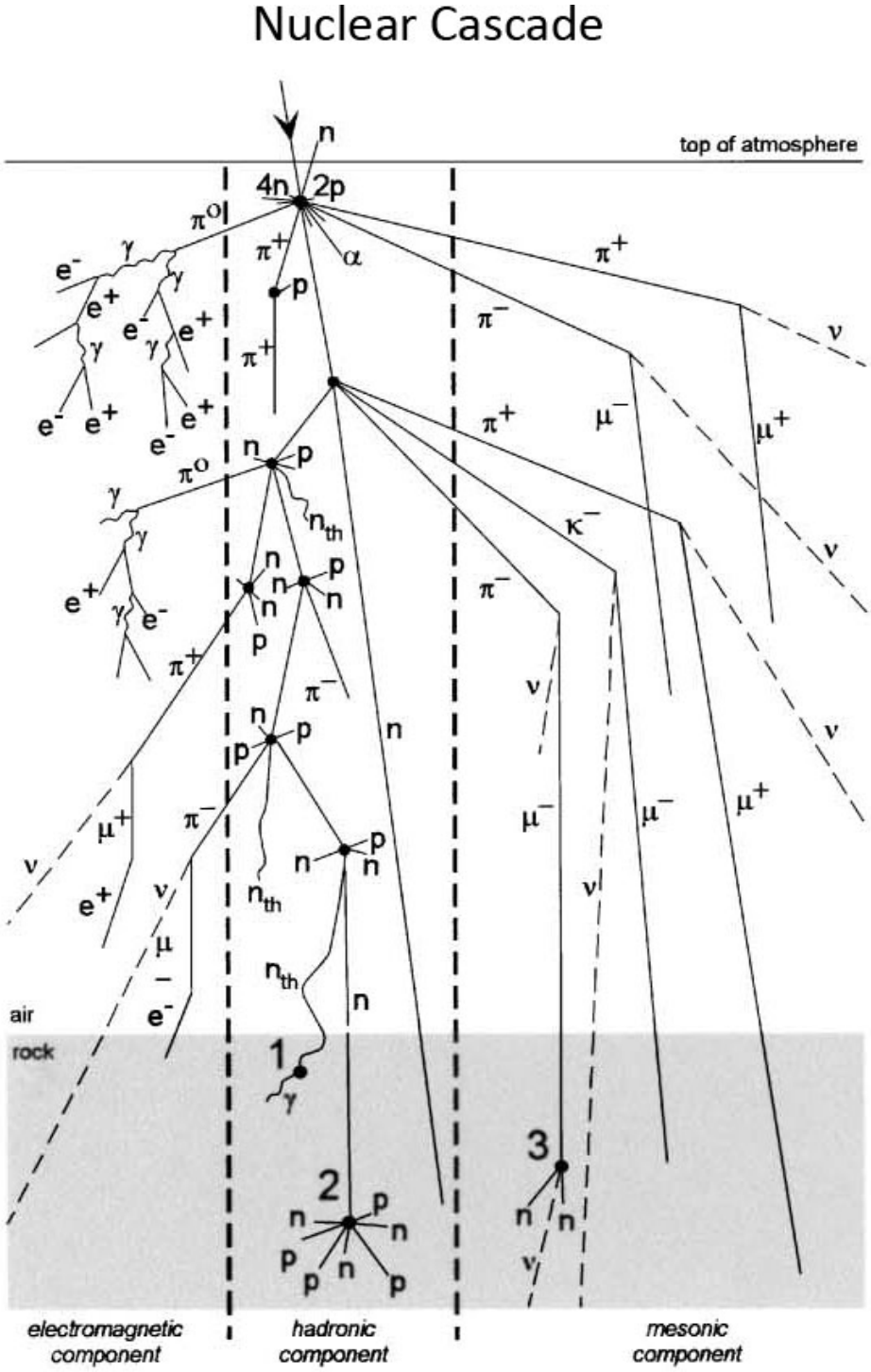

Figure 4: Nuclear cascade modified from Gosse and Phillips, 2001.

producing pions. Pions then decay to muons. Their small mass makes them less reactive than nucleonic particles and allows them to reach the earth's surface and become the dominant producer of nuclides at great depth below the earth's surface. Stopped negative muons can be captured by the electron shell of atoms and eventually be captured by the nucleus. This releases energy causing nuclear evaporation, expelling alpha particles, and producing cosmogenic nuclides. Muons can interact spallogenically. Combined with negative muon capture they account for ~2% of ^{10}Be production in rocks at sea level, high latitude. The interactions of muons and their contributions to nuclide production are poorly understood (Dunai, 2010; Gosse and Phillips, 2001). Nuclear decay can also produce cosmogenic nuclides but only need be taken into consideration with rocks containing considerable radioactive minerals (Dunai, 2010; Gosse and Phillips, 2001). Dating of objects older than 2-3 times the half life of the nuclide is not possible. At this point, the decay of the nuclide equals the production rate (saturation), producing the age of saturation (Dunai, 2010; Gosse and Phillips, 2001).

TCN ^{10}Be was used to date glacial landforms and create a chronology of glacial events in Francis Canyon and the Tamarack Bench during the summer of 2010. Sample collection procedure was based on Gosse and Phillips (2001) and Dunai (2010).

Glacial moraines are the result of debris transport entrained supraglacially and subglacially. Supraglacial debris is incorporated into the glacier from avalanches or rock fall from the surrounding canyon walls. Subglacial debris is entrained through basal plucking by melting and refreezing. This fractures, separates, and then incorporates

debris in the base of the glacier. Surface and basal debris is then transported to the snout or sides of the glacier forming lateral/frontal moraines. Moraines extend from the equilibrium line altitude (ELA) to the ablation zone (Evans, 2005) where accumulation terminates and deposition begins. The age of a boulder resting on a moraine crest is taken to represent the last time glacial deposition took place.

Spalling due to fire has a profound effect on the build-up of in-situ cosmogenic nuclides. Fire spalling is the loosening and removal of large pieces of surface rock through uneven heating and thermal expansion of material and vaporization of endolithic moisture (Bierman and Gillespie, 1991). Production rates of ^{10}Be decrease exponentially with depth (Gosse and Phillips, 2001). The problem is the removal of the TCN from the surface of the rock with the spalling resetting surface exposures toward younger age.

Anomalously young ages can also result from exhumation post deposition, removal of surface TCN by erosion, and snow shielding. Significant snow shielding can protect surfaces from cosmogenic ray exposure. The oldest ages in a sample set are considered closest to the actual exposure age of the landform since there is no guarantee that fire spallation, erosion, and snow shielding has not occurred.

Boulders may inherit nuclides from previous exposure if disintegration from avalanching and abrasion is insufficient to reset the cosmogenic clock (Owen *et al.*, 2002). Previous exposure history may also remain through reworking of old moraines yielding anomalously old age (Porter and Swanson, 2008).

Figure 5: Sample boulder.

The effects of fire, snow shielding, and erosion are mitigated through sample selection in the field. The effects of fire spalling can be reduced by sampling at elevations not affected by fire (Bierman and Gillespie, 1991). All moraines sampled are located at subalpine elevation (3000 – 3500 m). Subalpine forests of the SN have infrequent fires due to stand structure (Fites-Kaufman *et al.*, 2007) and should therefore have minimal fire history.

Only the largest granitic boulders (>2 m in diameter) were selected from the crest of moraines (Figure 5, pg. 21). Tall boulders on crests are selected because they are: less likely to be affected by fire spalling because the higher surface is farther away from the fuel, most likely to be windswept and therefore less susceptible to snow

shielding, less likely to have been exhumed by erosion, and subject to down slope transport or change in orientation since deposition.

Boulders sampled were photographed to show orientation (Figure 5). GPS locations were recorded to be used for spatial analysis and nuclide production rate calculation. Strike and dip of boulder surfaces, and horizons at every 45° increment (Table 2, pg. 23) off of north were measured using a Brunton geologic compass to quantify shading. The Top 5 cm of boulders totaling ~1kg of material was removed from the surface of quartz rich boulders using a 4 lb. sledge hammer and chisel. Boulders were identified according to Geological Survey Professional Paper 470 and classified as Round Valley Peak Granodiorite, Tungsten Hills Quartz Monzonite, and Wheeler Crest Quartz Monzonite with a density of ~2.65g/cm^3. The monzonites were only separable by geography. The source of the Wheeler Crest Quartz Monzonite was topographically segregated and could only appear on the Tamarack Bench or the Tamarack Lakes drainage.

Based on mapping, morphostratigraphy, and the current accepted framework of SN glacial chronology (Table 3, pg 23), four moraines were selected, two from Francis Lake Canyon (FCm1 and FCm2), and two from Tamarack Bench (FLm2 and TBm2). FCm4 is the outer most terminal moraine of the first glacial moraine series from the Francis cirque. Dating the outer terminal provides a maximum age constraint on the FCm4 advance. The lateral portion of this moraine was sampled due to lack of appropriate

Table 2 Cosmogenic field data.

ID	Map ID	UC Lab Label	Latitude (DD)	Longitude (DD)	Field Photo #	Strike °	Dip °	N	45°	90°	135°	180°	225°	270°	315°	Shielding Correction	Elevation (m)	Thickness (mm)	Rind (mm)	Lab Photo #	Rock Type
TB-10-FL2f	FLm2	DK-1	37.4438	-118.6870	145146	188	28	1	10	11	10	10	16	10	5	0.9797	3161	58	6	32, 031	RVP granodiorite
TB-10-FL2g	FLm2	DK-2	37.4438	-118.6870	147-149	124	44	1	10	9	10	11	15	13	4	0.9224	3161	76	5	34, 033	RVP granodiorite
TB-10-FL2h	FLm2	DK-3	37.4438	-118.6871	150-152	108	43	0	9	9	9	10	14	14	4	0.9274	3161	140	8	36, 035	RVP granodiorite
TB-10-FL2i	FLm2	DK-4	37.4436	-118.6871	153-154	162	37	0	7	10	10	11	14	11	1	0.9543	3162	70	9	38, 037	RVP granodiorite
TB-10-FL2j	FLm2	DK-5	37.4436	-118.6872	155-157	135	19	2	8	9	11	9	15	11	3	0.9923	3162	54	3	40, 039	RVP granodiorite
TB-10-2f	TBm2	DK-6	37.4542	-118.6851	75-76	30	9	3	10	9	5	5	8	8	0	0.9987	3109	92	7	41, 042	RVP granodiorite
TB-10-2g	TBm2	DK-7	37.4541	-118.6853	77-79	334	26	2	7	9	5	6	6	5	0	0.9853	3108	71	6	44, 043	RVP granodiorite
TB-10-2h	TBm2	DK-8	37.4543	-118.6851	80-82	55	24	0	9	7	5	6	5	7	0	0.9884	3113	60	N/A	45	RVP granodiorite
TB-10-2i	TBm2	DK-9	37.4545	-118.6856	83-85	315	11	2	6	7	5	6	5	5	0	0.9989	3111	50	15	46, 047	RVP granodiorite
TB-10-2j	TBm2	DK-10	37.4549	-118.6852	86-87	269	23	-1	6	6	6	6	6	6	2	0.9902	3113	101	3	49, 048	RVP granodiorite
FC-10-4f	FCm4	DK-11	37.4246	-118.7044	110-111	257	22	-1	-1	10	16	13	19	15	9	0.9881	3565	25	4	10, 009	TH qtz monzonite
FC-10-4g	FCm4	DK-12	37.4246	-118.7038	112-113	226	55	-1	0	10	16	13	15	18	12	0.8533	3566	33	7	8, 007	TH qtz monzonite
FC-10-4h	FCm4	DK-13	37.4246	-118.7035	114-115	189	18	-1	0	9	14	10	20	16	12	0.9898	3562	29	5	6, 005	TH qtz monzonite
FC-10-4i	FCm4	DK-14	37.4243	-118.7032	116-117	221	27	-2	0	6	15	12	21	21	12	0.9756	3570	40	10	4, 003	TH qtz monzonite
FC-10-4j	FCm4	DK-15	37.4243	-118.7031	118-120	248	14	-2	0	9	13	13	21	21	10	0.9899	3574	32	4	1, 002	TH qtz monzonite
FC-10-5Lf	FCm3	DK-16	37.4299	-118.7109	121-122	102	15	0	0	15	17	10	9	10	5	0.9936	3467	100	12	23, 022	TH qtz monzonite
FC-10-5Lg	FCm3	DK-17	37.4296	-118.7106	123-124	130	14	0	0	15	17	10	9	10	5	0.9943	3473	63	6	25, 024	RVP granodiorite
FC-10-5Lh	FCm3	DK-18	37.4295	-118.7107	125-126	300	31	0	0	11	15	11	7	11	5	0.9737	3474	40	3	26	RVP granodiorite
FC-10-5Li	FCm3	DK-19	37.4297	-118.7108	127-128	238	56	-1	0	10	15	12	9	11	5	0.8491	3471	52	8	28, 027	RVP granodiorite
FC-10-5Lj	FCm3	DK-20	37.4298	-118.7108	129-131	57	21	0	0	11	17	10	10	11	6	0.9896	3469	45	8	30, 029	RVP granodiorite
		Blank 1																			
		Blank 2																			

Table 3 Summary of late Pliestocene/Holocene Sierran glacial chronology. *date correlated here to stage name

Glacial Stage	Age (ka)	Methods	Location	Study
Matthes	1885	Sketches	Mt. Lyell	Russell, 1885
Recess Peak	13.1/13.5	$^{14}C/^{36}Cl$	Bishop Creek	Clark and Gillespie, 1997/Phillips et al., 2009
Tioga4	16-14.5	^{36}Cl	Bishop Creek	Phillips et al., 2009
Tioga3	18.5-17	^{36}Cl	Bishop Creek	Phillips et al., 2009
Tioga 2	25-20	^{36}Cl	Bishop Creek/Bloody Canyon/Chiatovitch	Phillips et al., 1996
Tioga1	28-24	^{36}Cl	Bishop Creek	Phillips et al., 2009
Tahoe	170-130/>119	$^{36}Cl/(^{40}Ar/^{39}Ar)$	Bishop Creek/Saw Mill Canyon (basalt flow)	Phillips et al., 2009/Gillespie et al., 1984*
Sherwin	>750	$^{40}Ar/^{39}Ar$	Big Pumice cut (Bishop Tuff)	Sarna-Wojcicki et al., 2000
McGee	<2600	K/Ar	McGee Mt.(McGee Mt. basalt)	Dalrymple, 1963

boulders on the terminal section. Dating FLm2 provides a date for the last time a glacier emerged from Francis Canyon. TBm2 is the terminal moraine for the final advance on the Tamarack Bench before the glacier enters Rock Creek Drainage (King, 2010). TBm2 provides maximum bounding age for the Tamarack Bench and completes the glacial sequence stratigraphy for Rock Creek.

Sample Preparation

The goals of sample preparation are to purify the quartz for analysis, concentrate the TCN, and transform it into a form appropriate for analysis (Gosse and Phillips, 2001). This is usually done in two stages: 1) a physical and chemical pretreatment phase which separates, concentrates, and purifies the target minerals; and 2) a phase which extracts the isotopes from the minerals and other none TCNs (Gosse and Phillips, 2001). TCN concentrations are measured using accelerator mass spectrometry (Reimer *et al.,* 2009; Finkel and Suter, 1993; Synal, 1995).

Samples were taken to the University of California, Riverside lab and steel brushed to remove organics, carbonate, and dust. They were chopped using a rock crusher, then ground up using a Chipmunk Crusher, a mortar and pestle, and sieved to 500-250 microns. Sieves, crushers, and mortar and pestle were all cleaned before starting a new sample. Sample preparation for AMS measurement was done at the University of Cincinnati under the direction of Dr. Lewis Owen. Targets were sent to the University of Purdue for AMS measurement.

Aqua Regia

Target mineral quartz was separated through physical and chemical isolation using aqua regia, frothing, magnetic separation, heavy liquid (LST) (density 2.7 g/mL), and hydrochloric acid (HCl)/ Nitric acid (HNO_3) and hydrofluoric acid (HF)/Nitric acid ($HNO_{3)}$ baths. Two hundred grams of each sample were placed in a clean, 1 L plastic bottle. Two hundred mL of HCl and 100 mL HNO_3 were combined (aqua regia), added to samples in the plastic bottles, and allowed to soak for 24 hours to remove metals, carbonates, phosphates, organics, and isobars. Acid mixture was poured off and samples rinsed in their bottles 3 times with tap water. This process was performed twice.

5% HF Leaching

Five percent HF leaching was used to etch/dissolve feldspars and etch quartz. The plastic bottles were then filled with 800 mL of 5% HF/HNO_3 and placed on heated rollers for ~24hrs. Acid was poured off and the sample rinsed with deionized water in the plastic container.

A second 5% HF/HNO_3 bath was used to dissolve remaining impurities and rinsed with deionized water. Once again samples were examined under a microscope.

Frothing

Samples were frothed to separate out feldspars and micas based on wetting properties using organic surfactants. The froth is a mixture of 1 L lauryl amine solution (1L deionized H_20, 1 g lauryl amine, 1 mL acetic acid), 4mL HF, 20 L water, and 4-5 drops of eucalyptus oil. Plastic bottles containing sample were emptied into a large stainless steel mixing bowl the frothing mixture was pressurized and sprayed vigorously over the sample to float micas and feldspars. The froth was quickly poured off removing micas and feldspars. This was repeated 3 times for each sample. Samples were rinsed and placed in clean, dry beakers in an oven to dry. A portion of each sample was examined under a microscope to check for impurities.

Magnetic Separation

A Frantz Isodynamic Separator, model L-1, was used to eliminate mineral grains susceptible to magnetics. A portion of each sample was checked under a microscope.

Mineral Separation (Heavy Liquids)

Heavy liquids were used to separate quartz from denser minerals, as well as to remove possible remaining feldspars with lower densities than quartz. Samples with minerals other than quartz were placed in 150 mL of heavy liquid (LST 2.75 g/cc) for density separation in a gravity separation funnel. Deionized water was added in steps to the solution in small amounts to gradually lower the density. After each addition of

water, the gravity separation funnel was shaken and allowed to resettle. Minerals with a greater density than quartz settled out and drained off. Water was continuously added until the quartz (2.65 g/cc) sank and the feldspars (2.55 g/cc) remained afloat. Quartz was then drained from the solution into a clean 1 L plastic bottle. Samples were rinsed with deionized water, oven dried, and checked for mineral composition.

1% HF Leaching

A 1% HF leach was used to remove meteoric components. Once pure quartz was obtained and verified, the plastic bottles containing sample were filled with 800 mL of 1% HF/HNO_3, placed on heated rollers for ~24hrs, and later rinsed with deionized water. Once again samples were placed in clean beakers and oven dried.

Dissolution

Clean Teflon beakers were tared on a Mettler AB 3044-S balance. Fifteen grams of pure quartz was added to each beaker. Plastic crucibles were tared in order to measure precise amounts of AMS targets ^{9}Be (LBC 12, 1354 ppm) and ^{25}Al (Spec Pure Alfa Aesar, 1000 µg/ml). These weights were recorded, and added to the quartz. The amount was noted to the nearest milligram. ^{9}Be and ^{25}Al should otherwise not be present in the samples. AMS analysis is reported in isotopic ratios of ^{9}Be/^{10}Be and ^{25}Al/^{26}Al. Dates are calculated from these ratios. It is important to be as accurate as possible. A mixture of HF and HNO_3 was added to each beaker to dissolve the quartz, so

that ^{9}Be and ^{25}Al can be counted with the ^{10}Be and ^{26}Al during AMS measurement. Amounts of HF and HNO_3 needed to dissolve the samples are determined by the mass of the quartz in each sample (volume of HF = 5 x qtz g, volume of HNO_3 = 3 x qtz g). The solution is then heated on a hot Plate in a fume hood for 6 hrs or until dissolved. 250 mL plastic bottles are tared on the balance and the quartz solution is placed in the bottle, weighed, and recorded. A 60 mL bottle is then tared and 10% of the sample removed from the 250 mL bottle to make an Al aliquot. The solution in the 250 mL bottle is then poured back into the Teflon beaker and placed on the hot Plate in the fume hood to evaporate the liquid.

Perchloric Fuming

Once evaporated the fluorides were fumed off using a mixture of perchloric acid ($HClO_4$) and nitric acid solution (H_2O/HNO_3, 1/1). Twenty mL of the nitric acid solution and 4 mL of the perchloric acid was added to the beakers and heated in a fume hood until dry. Once dry the sides of the beaker were rinsed using deionized water. Two mL of perchloric acid was again added and swirled to dissolve the entire sample. Sample was placed on the hot Plate and fumed until dry. This step was performed twice. Six mL of 9 N HCl was added while the beaker was still warm. The dissolved sample was pipetted into a 15 mL test tube. Beaker was rinsed with 1 mL of deionized water and pipetted into the same test tube.

Anion Columns

Anion columns were used to separate the anion fraction from the cation fraction (beryllium portion). Columns containing resin were first conditioned by running through 60 mL of 9 N HCl. A new, clean Teflon beaker was placed under each column. Sample was pipetted from the test tube directly into the column and allowed to drain into the beaker. Thirty-four mL of 9 N HCl was added and allowed to completely drain through the column into the beaker. The beaker was removed and placed on a hot Plate to dry. As soon as the sample was dry, 1 mL of 6 mL HCl is added while beaker was still warm. One drop of H_2O_2 was added. Dissolved sample was pipetted into a new 15 mL test tube. The beaker was rinsed with 5 mL of deionized water and pipetted into the same test tube. The beaker is saved and reused for the cation columns. Anion reject fractions were collected and stored in 125 mL plastic bottles by draining 80 mL of 0.1 N HCl through the columns.

Cation Columns

Cation columns separate the different cation fractions Ti, Be, and Al. The Ti fraction was separated and stored in a 125 mL bottle by pipetting the sample directly into the column, then draining 80 mL of 1 N HCl through the column and into the bottle. The Be fraction was separated into the Teflon beaker used in the anion column portion by draining 80 mL of 1N HCl through the column. The beaker was then placed on a hot Plate to dry. Once dry, 1 mL of 6 N HCl and one drop of H_2O_2 was added to the beaker

while it was still warm. The dissolved sample was pipetted into a new 15 mL test tube. The beaker was rinsed with 1 mL of deionized water and pipetted into the same test tube. The Be reject fraction was separated and stored in 250 mL plastic bottles by draining 120 mL of 1 N HCl through the column into the bottle. Al was separated next by draining 80 mL of 2.5 N HCl through the column and into a new 125 mL plastic bottle and stored. The cation columns were then conditioned by draining 200 mL of 6 N HCl and then a subsequent 60 mL of deionized water through each column.

Precipitation of Be

Beryllium was precipitated from the cation beryllium solution. One mL of 1:1 NH_4OH:H_2O was added to the sample and shaken gently to mix. This allows the Be to precipitate. The test tube was vortexed for 2-3 seconds and allowed to stand for 10 minutes.

Rinsing Plugs

The beryllium gel was rinsed to remove NH_4OH before drying. After being in a standing position for 10 minutes the samples are vortexed again for 2-3 seconds and centrifuged for 2 minutes. The liquid was decanted into a glass beaker in the fume hood. 3 mL of deionized water was added to the test tube, vortexed for 2-3 seconds, centrifuged for 2 minutes, and again decanted into the beaker. Samples were rinsed in this manner 3 times each. No more liquid was added after the final decanting.

Drying

The beryllium gel was dried to prep samples for targeting. Be gel was pipetted from the test tubes into a clean quartz crucible. Test tubes were rinsed with 1-2 drops of deionized water and pipetted into the crucible. The crucible was placed into an incubator and allowed to dry for 24 hrs.

Oxidizing

The dried samples were then oxidized in an oven at 750°C. Each sample is taken from the incubator to the holding block with metal tweezers and covered with individual glass lids. The holding block is then placed in the oven until it reaches 750°C. The block was then removed and the quartz crucibles were uncovered and placed in slightly larger plastic crucibles and labeled.

Loading Cathodes

Samples were then ready to be loaded into targets for AMS measurement. Drill blanks were cleaned by sanding and cleaning with isopropyl alcohol. Clean targets were placed on foil in the preset targeting station. The quartz crucible was then removed from the plastic crucible with a clean drill blank. The sides of the crucible are scraped to remove all beryllium crystals from the sides. Each sample was ground into a fine powder. An equal amount of niobium powder was added using a curette. The sample was mixed and dumped into the crucible on top of the cathode and guided into the

hole. A drill blank and hammer were used to tamp the powder. The cathode was placed upside-down into a clean plastic crucible. Cathode number and sample name were recorded.

Calculations

Calculations were performed using the CRONUS-Earth (Cosmic-Ray Produced Nuclide Systems networks) online calculator version 2.2 which is based on MATLAB software. The CRONUS-Earth project is an initiative to improve Earth science applications of cosmogenic-nuclide geochemistry. This project also collaborates with CRONUS-EU, a similar initiative funded by the European Union. The online calculator was created with the purpose of calculating exposure ages, comparing previously published exposure ages via standardization, and evaluate the sensitivity of results to differences between published production rate scaling schemes. The goal is an internally consistent result that reflects the current accepted practices. Using current accepted practices means that ages calculated will change through time due to improvements made in the understanding of the physics behind production of cosmogenic nuclides and the coverage of production rate calibration measurements. The exposure age calculator keeps internal consistency by ensuring that the exposure ages are generated with the same scaling scheme used in creating the reference production rate from the set of calibration measurements as was used to scale the reference production rate. For specifics on the interworking of the calculator see Balco *et al*. (2008).

Accuracy and precision are based on the following sources of uncertainty: analytical/observational (1-5%), methodological (5-15%), geological/natural (0-100%) (Table 1). Observed quantities such as sample thickness, surface geometry, topographic shielding, elevation, sample weighing, and AMS measurements are examples of analytical/observational. Methodological includes the radionuclide half-life, SLHL-production rate, cosmic ray flux attenuation in rocks, and scaling factors 10% uncertainty (Dunai, 2010). This is important because exposure ages cannot be known more accurately than the production rates (Balco *et al.*, 2008). Geological/natural sources include: erosion rates, shielding corrections (snow), and pre-exposure. Reporting internal uncertainty only accounts for uncertainty of the AMS measurement and should be used only to compare ages within a sample landform (boulders on a moraine). External error includes the spallation and muon production uncertainties due to production rate scaling which includes uncertainty associated with input parameters through scatter of the scaled production rates (Balco *et al.*, 2008). The scatter of a population of samples is used to assess the effect of erosion, spalling, and pre-exposure. The variance of a population is used to constrain the maximum analytical uncertainty (Gosse and Phillips, 2001).

Data from a ^{10}Be study of San Gorgonio in the San Bernadino Mountains of southern California (Owen *et al.*, 2003) has been recalculated using this system to

Table 4 Cronus calculator inputs.

Daryl Kohut Master's Thesis Data - Francis Canyon/Tamarack Bench, Sierra Nevada, California 2011.

Sample name	Latitude	Longitude	Elevation	Elv/pressure	Thickness	Density	Shielding	Erosion rate	[Be-10]	+/-	Be AMS	[Al-26]	+/-	Al AMS
	(DD)	(DD)	(m)	flag	(cm)	(g cm-2)	correction	(cm yr-1)	atoms g-1	atoms g-1	standard	atoms g-1	atoms g-1	standard
DK1	37.44375	-118.687	3161	std	5.8	2.65	0.9796992	0	4.3162E+05	1.1607E+04	07KNSTD	0.00E+00	0.00E+00	KNSTD
DK2	37.44375	-118.687	3161	std	7.6	2.65	0.9223565	0	4.5171E+05	1.6995E+04	07KNSTD	0.00E+00	0.00E+00	KNSTD
DK3	37.44375	-118.687	3161	std	14	2.65	0.9274498	0	5.4400E+05	1.9424E+04	07KNSTD	0.00E+00	0.00E+00	KNSTD
DK4	37.44364	-118.687	3162	std	7	2.65	0.9543398	0	5.3576E+05	1.3046E+04	07KNSTD	0.00E+00	0.00E+00	KNSTD
DK5	37.44361	-118.687	3162	std	5.4	2.65	0.9922965	0	5.7701E+05	1.5760E+04	07KNSTD	0.00E+00	0.00E+00	KNSTD
DK6	37.45417	-118.685	3109	std	9.2	2.65	0.9987023	0	6.5886E+05	1.6398E+04	07KNSTD	0.00E+00	0.00E+00	KNSTD
DK7	37.45414	-118.685	3108	std	7.1	2.65	0.9853036	0	3.2322E+05	1.2143E+04	07KNSTD	0.00E+00	0.00E+00	KNSTD
DK8	37.45428	-118.685	3113	std	6	2.65	0.9884358	0	6.0116E+05	1.6162E+04	07KNSTD	0.00E+00	0.00E+00	KNSTD
DK9	37.4545	-118.686	3111	std	5	2.65	0.9989092	0	6.2220E+05	1.7452E+04	07KNSTD	0.00E+00	0.00E+00	KNSTD
DK10	37.45489	-118.685	3113	std	10.1	2.65	0.9902027	0	8.0133E+05	2.1658E+04	07KNSTD	0.00E+00	0.00E+00	KNSTD
DK11	37.42458	-118.704	3565	std	2.5	2.65	0.9881076	0	1.7753E+06	5.0738E+04	07KNSTD	0.00E+00	0.00E+00	KNSTD
DK12	37.42456	-118.704	3566	std	3.3	2.65	0.8533169	0	4.1419E+06	1.0326E+06	07KNSTD	0.00E+00	0.00E+00	KNSTD
DK13	37.42458	-118.704	3562	std	2.9	2.65	0.989753	0	2.0683E+06	1.7559E+06	07KNSTD	0.00E+00	0.00E+00	KNSTD
DK14	37.42433	-118.703	3570	std	4	2.65	0.9756444	0	1.7571E+06	4.3189E+05	07KNSTD	0.00E+00	0.00E+00	KNSTD
DK15	37.42425	-118.703	3574	std	3.2	2.65	0.9898612	0	8.4817E+05	4.6099E+05	07KNSTD	0.00E+00	0.00E+00	KNSTD
DK16	37.42992	-118.711	3467	std	10	2.65	0.9935811	0	4.8661E+05	1.1997E+05	07KNSTD	0.00E+00	0.00E+00	KNSTD
DK17	37.42964	-118.711	3473	std	6.3	2.65	0.9942635	0	5.5348E+05	1.8669E+05	07KNSTD	0.00E+00	0.00E+00	KNSTD
DK18	37.42953	-118.711	3474	std	4	2.65	0.9737076	0	5.5941E+05	2.1813E+04	07KNSTD	0.00E+00	0.00E+00	KNSTD
DK19	37.42972	-118.711	3471	std	5.2	2.65	0.8491019	0	6.1849E+05	1.6082E+04	07KNSTD	0.00E+00	0.00E+00	KNSTD
DK20	37.42983	-118.711	3469	std	4.5	2.65	0.989577	0	2.5941E+06	1.8590E+06	07KNSTD	0.00E+00	0.00E+00	KNSTD
Blank 1	0	0	0	std	0	2.65	1	0	0.0000E+00	0.0000E+00	07KNSTD	0.00E+00	0.00E+00	KNSTD
Blank 2	0	0	0	std	0	2.65	1	0	0.0000E+00	0.0000E+00	07KNSTD	0.00E+00	0.00E+00	KNSTD

update the ages with new production rates and half-life measurements. This study was selected because it is the southwestern margin of quaternary glaciation in North America (Owen *et al.*, 2003) and it is in close proximity to our study area. Recalculations can be done as long as the necessary input parameters are available (Table 4, pg. 34). Inconsistencies may arise from two input parameters from studies performed by different investigators, shielding correction factor and Be concentrations calculations. Both of these parameters are necessary inputs for the online calculator and therefore are calculated outside the actual age calculation. The errors of these inputs can be estimated based on the spread of the age population (Balco *et al.*, 2008).

Ages were calculated from the ratios of $^{10}Be/^{9}Be$ measured by PRIME Lab at Purdue University. First ratios were corrected for blanks by subtracting out its ratio. Next, the ratios were converted to concentrations based on the measured amounts of known ^{9}Be carrier added previously to the samples. This was done by dividing the $^{10}Be/^{9}Be$ ratio by the weight of the quartz, then multiplying by the number of ^{9}Be atoms. This provides a concentration in atoms/gram. This calculation is then added to a spreadsheet downloaded from the CRONUS website (http://hess.ess.wash-ington.edu/math/) along with other measured parameters. The measured parameters consist of: sample name, latitude, longitude, elevation, thickness, density, shielding correction, erosion rate, ^{10}Be concentration, ^{10}Be measurement error, and Be AMS standard. Shielding correction was calculated using the CRONUS shielding calculator which uses horizon measurements describing the surrounding canyon walls made in the

Table 5 Cronus calculator results.									
Scaling scheme for spallation Lal(1991) and Stone(2000), results not dependent on spallogenic production rate model.									
Sample name	Map Id	Field Label	Thickness scalling factor	Shielding factor	Production rate (muons) (atoms/g/yr)	Internal Uncertainty (yr)	Exposure age (yr)	External Uncertainty (yr)	Production rate (spallation) (atoms/g/yr)
DK6	TBm2	TB-10-2f	0.9275	0.9987	0.465	464	18554	1684	35.21
DK7	TBm2	TB-10-2g	0.9434	0.9853	0.468	341	9054	859	35.31
DK8	TBm2	TB-10-2h	0.9519	0.9884	0.47	449	16621	1518	35.85
DK9	TBm2	TB-10-2i	0.9597	0.9989	0.471	476	16908	1550	36.48
DK10	TBm2	TB-10-2j	0.9208	0.9902	0.464	622	22892	2094	34.74
Average						470	16806	1541	
DK1	FLm2	TB-10-FL2f	0.9535	0.9797	0.477	315	11676	1065	36.6
DK2	FLm2	TB-10-FL2g	0.9396	0.9224	0.474	497	13164	1250	33.95
DK3	FLm2	TB-10-FL2h	0.8925	0.9274	0.465	595	16606	1566	32.43
DK4	FLm2	TB-10-FL2i	0.9442	0.9543	0.475	367	15022	1360	35.32
DK5	FLm2	TB-10-FL2j	0.9566	0.9923	0.477	421	15369	1405	37.21
Average						439	14367	1329	
DK16	FCm3	FC-10-5Lf	0.9216	0.9936	0.511	2792	11291	2960	42.71
DK17	FCm3	FC-10-5Lg	0.9496	0.9943	0.518	4202	12420	4339	44.19
DK18	FCm3	FC-10-5Lh	0.9676	0.9737	0.523	492	12571	1201	44.12
DK19	FCm3	FC-10-5Li	0.9581	0.8491	0.52	421	16108	1466	38.03
DK20	FCm3	FC-10-5Lj	0.9636	0.9896	0.521	42489	58428	42800	44.53
Average						1977	13700	2335	
DK11	FCm4	FC-10-4f	0.9796	0.9881	0.54	1072	37175	3431	47.66
DK12	FCm4	FC-10-4g	0.9732	0.8533	0.538	26222	102507	27767	40.91
DK13	FCm4	FC-10-4h	0.9764	0.9898	0.539	37352	43521	37547	47.5
DK14	FCm4	FC-10-4i	0.9676	0.9756	0.537	9334	37619	9900	46.61
DK15	FCm4	FC-10-4j	0.974	0.9899	0.54	9640	17658	9762	47.71

Table 6 Cronus calculator results.										
Exposure ages time-varying production models.										
Scaling scheme for spallation:	**Desilets et al. (2003, 2006)**		**Dunai (2001)**		**Lifton et al. (2005)**		**Time-dependent Lal (1991)/Stone (2000)**			
Sample name	Exposure age (yr)	External Uncertainty (yr)	Exposure age (yr)	External Uncertainty (yr)	Exposure age (yr)	External Uncertainty (yr)	Exposure age (yr)	External Uncertainty (yr)	**Map Id**	**Field Label**
DK6	17413	2108	17283	2083	16909	1726	18048	1593	TBm2	TB-10-2f
DK7	8578	1064	8642	1067	8315	879	8849	818	TBm2	TB-10-2g
DK8	15702	1907	15626	1889	15259	1565	16254	1444	TBm2	TB-10-2h
DK9	15959	1942	15875	1923	15507	1595	16520	1474	TBm2	TB-10-2i
DK10	21238	2583	20992	2542	20595	2116	22059	1963	TBm2	TB-10-2j
DK1	11068	1342	11095	1340	10741	1100	11471	1018	FLm2	TB-10-FL2f
DK2	12490	1551	12493	1545	12123	1283	12958	1200	FLm2	TB-10-FL2g
DK3	15640	1934	15565	1917	15196	1599	16238	1492	FLm2	TB-10-FL2h
DK4	14220	1718	14185	1707	13811	1407	14756	1299	FLm2	TB-10-FL2i
DK5	14533	1765	14490	1753	14119	1449	15084	1341	FLm2	TB-10-FL2j
DK16	32086	3924	31447	3829	30950	3201	34465	3094	FCm3	FC-10-5Lf
DK17	85496	24089	83213	23413	81658	22344	92841	25008	FCm3	FC-10-5Lg
DK18	36915	31934	36188	31296	35623	30718	39526	34056	FCm3	FC-10-5Lh
DK19	32424	8911	31774	8724	31273	8347	34837	9132	FCm3	FC-10-5Li
DK20	16098	8989	16003	8934	15607	8655	17192	9496	FCm3	FC-10-5Lj
DK11	10466	2868	10505	2876	10142	2700	11077	2894	FCm4	FC-10-4f
DK12	11506	4123	11527	4129	11149	3929	12208	4257	FCm4	FC-10-4g
DK13	11650	1451	11668	1447	11285	1199	12358	1151	FCm4	FC-10-4h
DK14	14877	1803	14823	1789	14430	1476	15761	1396	FCm4	FC-10-4i
DK15	48537	35681	47427	34852	46249	33845	52694	38527	FCm4	FC-10-4j

Figure 6: FCm4 facing southwest.

field. This spreadsheet was then uploaded to the calculator. Ages are given along with internal and external errors with 1σ uncertainty for multiple scaling schemes. The scaling scheme used was Lal (1991)/Stone (2000) because it does not include a geomagnetic correction through time (Table 5, pg. 36). This is poorly understood and can introduce unnecessary error. However, the results of the other time dependent scaling schemes are reported (Table 6, pg. 37). Erosion rate was considered zero because the boulders exhibited little evidence of surface erosion. An estimation of the erosion rate would also introduce unnecessary uncertainty and error.

TCN ^{10}Be was used to create the chronology of glacial advances using the Lal (1991)/Stone (2000) time independent production model. The effects of erosion

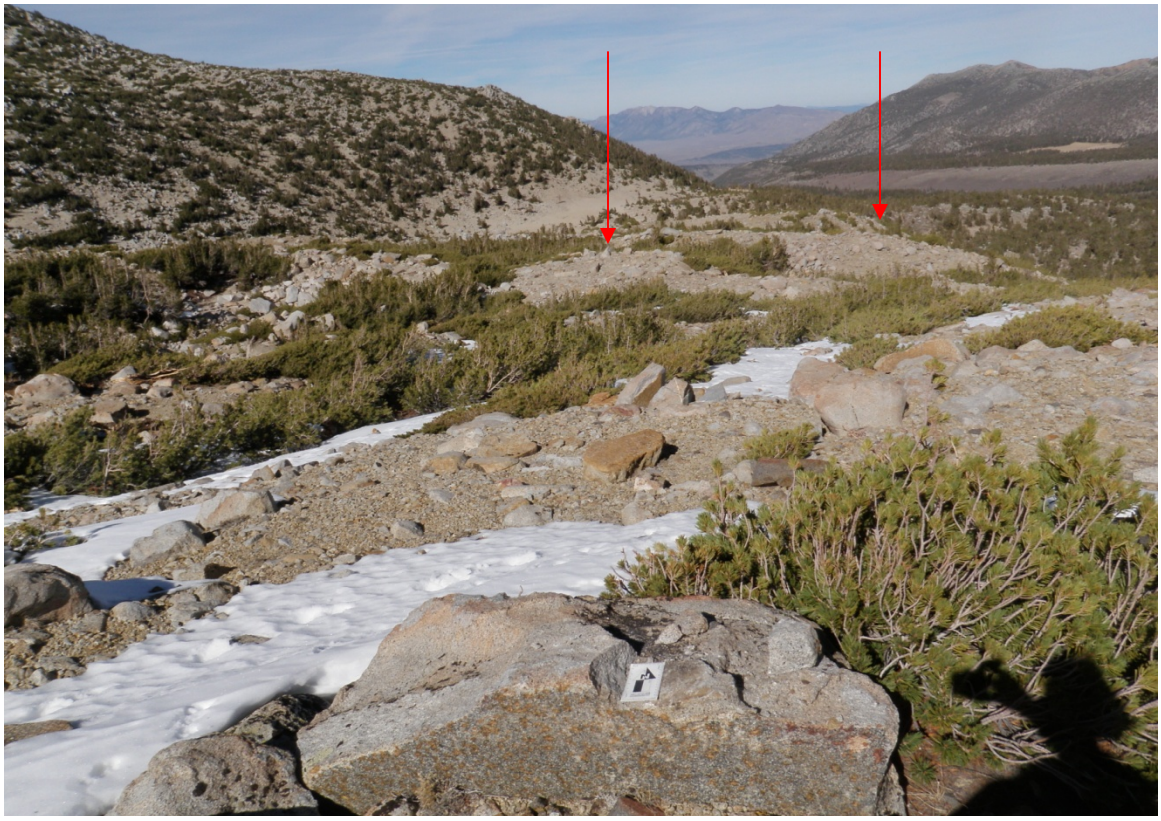

Figure 7: FCm3 terminus and hummocky features.

exposing fresh boulders of the sampled moraines should minimal in this study. Over ~20 ka less than 1 m of soil would be eroded (Phillips *et al.*, 2009). Of the 5 samples taken from FCm4 at an elevation of ~3560 m, 3 (DK-12, 13, 14) were not publication quality due to low current and large internal uncertainty (Table 5, red). The remaining two samples (DK-11, 15) also had significantly large internal uncertainties and the ages were in contradiction to the moraine's stratigraphic position and cross cutting relationships. The ages are reported but were not considered further. FCm4's position in the canyon (Figure 6, pg. 38) makes it vulnerable to rock fall and avalanching as a source of pre-exposure inheritance.

FCm3 samples (~3470 m) were taken from a lateral moraine. Left lateral, right lateral, or medial moraine could not be determined with certainty due to the ambiguity of position (Figure 7, pg. 39). The ages cannot be inferred as bounding, only depositional because of the ambiguity. FCm3 had one sample (DK-20) with low current and large internal uncertainty that was not publication quality and therefore reported but excluded from consideration. Sample DK-16 had low current, large uncertainty, but the ratio was considered reliable and therefore used in analysis (Table 5, yellow).

A plot of 2σ standard deviation was created to check for outliers in the data set (Figure 8, pg. 41). Young outliers would indicate fire spalling and or significant surface erosion. Old outliers suggest reworking of previously exposed material. The ages were plotted by glacial landform using Excel. A best estimate age was created based on the following criteria: exclusion of outliers, low internal uncertainty, low external uncertainty, limited self shielding, low snow cover, oldest age within the 2σ standard deviation grouping. An average age of each landform was calculated including outliers. Age models were cross plotted to show differences. All recalculated ages were also plotted, averaged, and interpreted in this manner.

Relative Dating Techniques

Relative dating is based on the idea that characteristics of weathering are time dependent and therefore reflect length of exposure (Birkeland *et al.*, 1979; Birman, 1964). The most consistent for delineating mapping units are granite weathering ratios

Figure 8: TCN Data Plots.

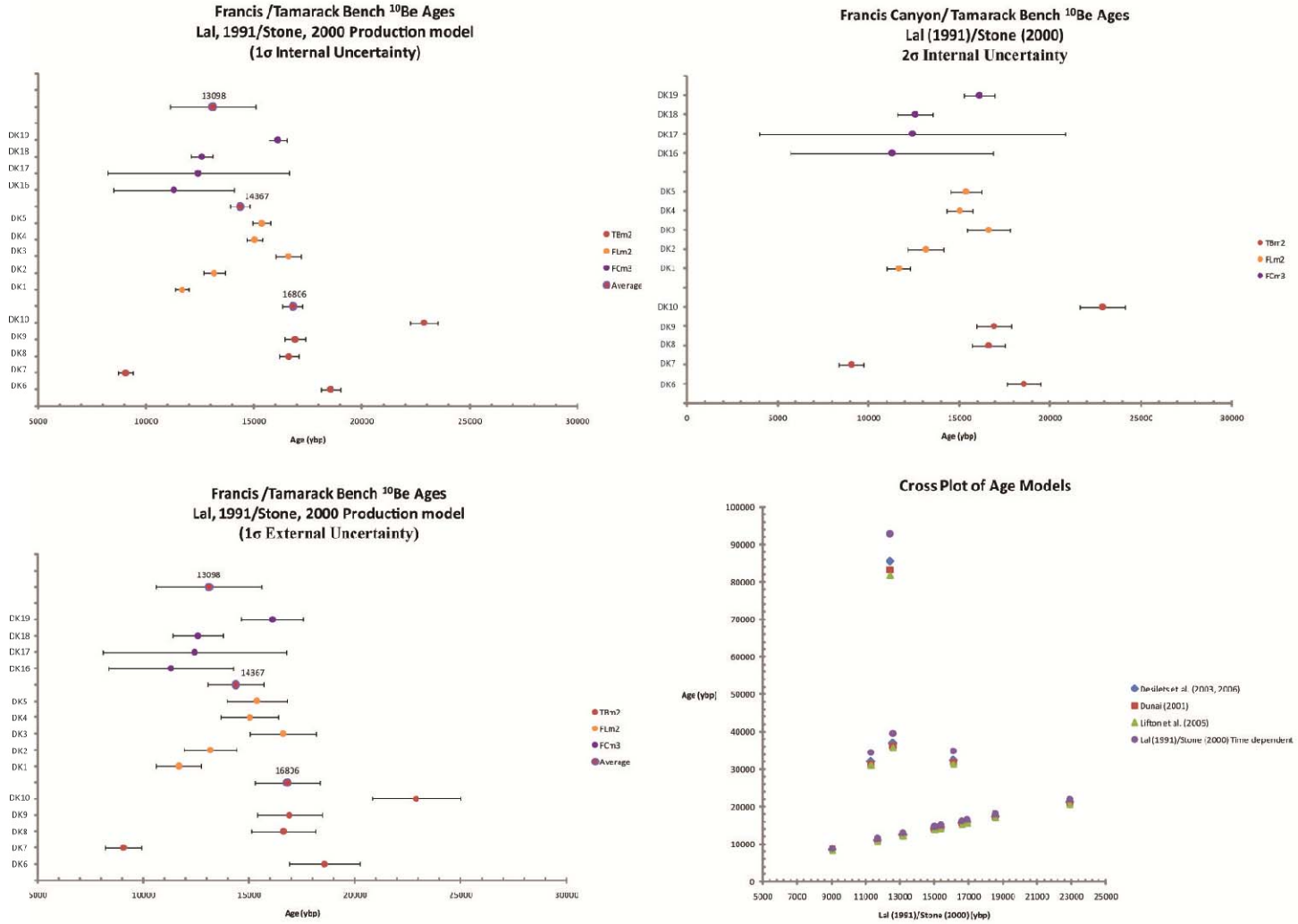

(GWRs), rind development, and subsurface weathering. Factors taken into account are vegetation cover (fire spalling), lithology (for consistent weathering), and location on the moraine (erosional transport) (Burke and Birkeland, 1979). Those used in this study are GWRs, rind development. In place of subsurface weathering, grain- size analysis of soils was used, modified from Sharp (1969).

Only boulders of granodiorite and quartz monzonite of similar grain size (2-4 mm) located on moraine crests were used. Similarities in composition and grain size help keep weathering rates from boulder to boulder consistent (Burke and Birkeland, 1979). Boulders located on moraine crests are less likely to have moved since deposition. Surrounding vegetation is considered because of the effects of fire.

Rind Thickness

Rind thickness was measured on all boulders sampled for TCN dating to quantify weathering, correlate it between advances, and support the cosmogenic ages. The rind was defined as a zone of discoloration on the surface of the boulder resulting from exposure. The greater the rind thickness, the longer the boulder has been exposed since deposition (Burke and Birkeland, 1979). Rinds were measured to the nearest mm. An average thickness was taken for each moraine and compared.

Granitic Weathering Ratio

Birman (1964) and Blackwelder (1931) demonstrated that granitic weathering ratios (GWR) can be used to delineate glacial advances within a drainage in the SN. Birman's (1964) methods were modified for this study. A granitic weathering ratio was generated by a count of 50 granitic boulders greater than 1 m in diameter classified by the counter to be either "fresh" or "weathered". A weathered boulder surface was defined as having >50% mineral grains with full grain relief. Boulders of similar lithology were selected to maintain comparable weathering rates. Counts were performed on the crests of moraines to help ensure the boulders were exposed since deposition and not recently exposed due to erosion or down slope transport. Two to three observers were used to reduce personal bias. Before counting, a practice count was performed by all counters to ensure agreement on the classification of weathered vs. fresh. Results were not shared until each observer had finished their counts. GWR's were presented as a percentage of fresh boulders for all counts taken on each moraine. Percent fresh boulders were calculated as follows:

$$\%F = \left(\frac{F}{F + W}\right) 100$$

Soil Grain-size Analysis

Grain-size in soil on the moraine crests was examined to assess whether landforms with increasing age contain a greater proportion of finer grains due to

Figure 9: Soil pit location.

cumulative weathering. These proportions should be comparable in landforms of similar lithology (Sharp, 1969a). Sharp's procedure was modified for soil grain-size analysis. Soil pits were dug on the crest of each of the moraines at locations which corresponded to the cosmogenic samples. Four pits were dug on the crest of each moraine (Figure 9, pg. 44). Soils were sampled at 15 and 30 cm using a small shovel. The samples were placed in plastic bags and brought to the lab and sieved to 4000, 2000, 500 and 63 microns according to the grain size divisions of the Wentworth Scale. Percentages of each grain size range were determined by total weight of the sample. An average of each grain size was calculated for each moraine at both depths. These averages were plotted for each glacial feature.

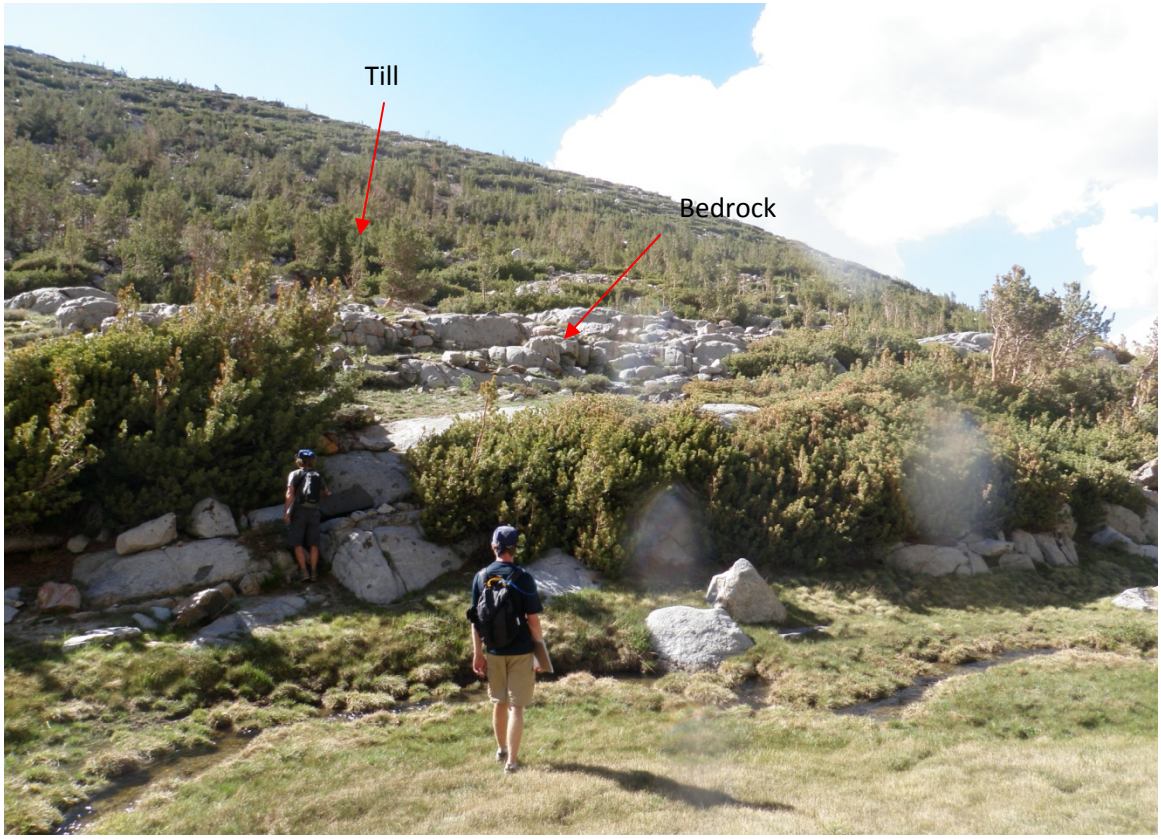

Figure 10: Contact of till/bedrock below FCm3.

Ex. $\%500\mu = \left(\frac{500\mu(g)}{TS(g)}\right)100$

Results

Mapping

Francis Canyon

Francis Canyon extends from an elevation of 3700 m to approximately 3170 m where it meets the Tamarack Bench. The canyon is about 506 m wide at the cirque headwall to 640 m at the canyon mouth. There are 6 moraine series preserved in Francis Canyon, 2 rock glacier deposits and 4 glacier deposits (map, Plate 1,). The majority of

Figure 11: Roche moutonees below Francis Lake.

the canyon floor is covered by glacier deposit. On the west side of the canyon is a prominent set of moraines perched on a Plateau ~100 m high. At a similar elevation perched on the east side of the canyon, is another smaller glacial deposit. The moraines were separated into 3 different units based on stratigraphy, morphology, and relative weathering characteristics, see unit descriptions for greater detail (map, Plate 1). To the east of the Plateau, ~1200 m below the headwall the glacier deposit is bounded by exposed bedrock and thin till veneer (Figure 10, pg. 45). This contact continues down canyon until buried by a landslide deposit that chokes the drainage between Plateau and canyon wall up and into Francis Lake. There is exposed bedrock on the east side just below the canyon wall in the form of 2 roche moutonees. The moutonees disappear under a thin veneer of till (Figure 11, pg. 46) that covers the rest of the canyon floor up to the confluence of Tamarack Bench. Fluvial deposits in Francis Canyon are limited and begin at the transition of glacial deposits to exposed bedrock and till. The source of the stream is the ice field on the cirque headwall. Much of the bedrock is likely exposed due to erosion by the stream which emerges from beneath the glacial deposit. Fluvium is

Figure 12: Blurred Plateau till/landslide contact (left); landslide contact with till (right).

deposited on top of bedrock and till. The landslide adjacent to Francis Lake lies on top of fluvium. Stream erosion has blurred the contact between the till from west Plateau wall and landslide (Figure 12, pg. 47). The contact of the landslide and till near Francis Lake shows the landslide post dates the till below the west Plateau (Figure 12). The stream then emerges onto a wider, flatter part of the canyon before entering Francis Lake. To the northeast of Francis Lake, just above the mouth of the canyon are valley wall rock glacier deposits. They appear to be the youngest glacial deposit near the mouth of the canyon, but no direct correlation could be made to other deposits.

Tamarack Canyon

Tamarack Canyon covers an elevation range of 3690 m to 3260 m from cirque headwall to canyon mouth at the confluence of the Tamarack Bench. It is ~540 m wide near the cirque and 1200 m wide at its mouth. There are two distinct rock glacier deposits located within 300 m of the headwall at ~3600 m elevation. Below this, glacial deposits exist as erratic boulders 1-3 m in diameter deposited on striated bedrock of

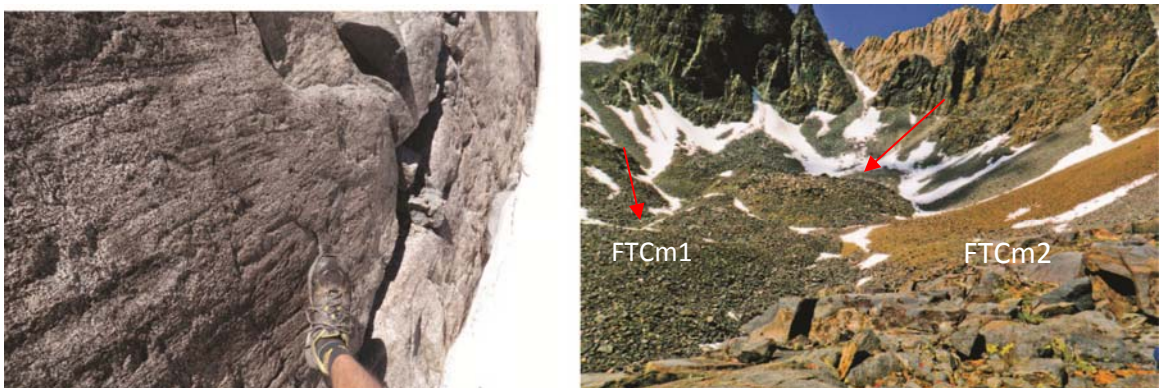

Figure 13: Bedrock striations Tamarack Canyon (left); FTCm1 and 2 (right).

granodiorite and diorite (Figure 13, pg. 48). Near the west and east canyon walls are several landslide and talus deposits that onlap bedrock indicating post glaciation. Beginning about 1800 m from the headwall of the cirque is a series of canyon wall rock glacier deposits which continue to the mouth of the canyon, and onlap the till deposits on the canyon floor. The rock glacier deposits appear to be the youngest glacial features at the mouth of the canyon and on the Tamarack Bench. Just to the west of the rock glacier deposits are 3 roche moutonees. These are oriented northeast indicating direction of ice flow. Near the mouth of the canyon is a series of fluvial deposits onlapping glacial till on the canyon floor. These deposits continue onto the Tamarack Bench as a series of interconnected streams and lakes.

Unit Descriptions

FTCm2 is the closest glacial deposit to the headwall of Francis Canyon cirque and is defined as a rock glacier deposit. It has a terminus ~40 m in height, lies at an elevation of ~3680 m, and displays no vegetation. This deposit is composed mostly of large (1-3 m

Table 7 Relative weathering characterisics of major glacial deposits. Francis/Tamarack Canyons.									
	FTCm2 (FC)	FTCm2 (TC)	FTCm1 (FC)	FTCm1 (TC)	FCm4	FCm3	FCm2	FLm2	TBm2
Elevation (m)	3680	3680	3650-3430	3660-3640	3650-3558	3550-3430	3550-3431	3160	3110
Height (m)	40	38	10	8	15	23	31	10	7
Slope %	77	72	NA	NA	50	32	36	NA	NA
GWR (%)	81	80	67	48	36	42	27	44	57
Soil (% silt/clay)	NA	NA	NA	NA	3	7	NA	7	9
^{10}Be age (ka)	NA	NA	NA	NA	NA	12.5	NA	16.6	18.5

diameter), angular granodiorite/diorite (~95%/10%) boulders with less than ~5% lichen coverage and 81% GWR. The glacial deposit is steep (77% slope), unstable, and slopes to the headwall. It is considered a rock glacier because of its continuous slope. A snow field was present in mid-summer at the back of the cirque, but no interstitial ice was found. Glacier deposits exhibit a depression after the moraine crest where the glacier ice once existed. This is the youngest deposit because it is found at the highest elevation in the canyon, and onlaps the next moraine (FTCm1), which lies at the base of the terminal moraine to the northwest. This moraine correlates from Francis to Tamarack Canyon based on similar elevations (3650-3430 m, 3660-3640 m) and height (10 m, 8 m) (Table 7, pg. 49). GWRs were significantly different (67%, 48%).

FTCm2 in Tamarack Canyon is a rock glacier deposit found at ~3680 m (Figure 14, pg. 49). Here FTCm2's terminal moraine is ~38 m high, composed of 80% fresh, angular, large boulders (1-3 m diameter) of basalt/diorite, and granodiorite (approximately 80%/20%), and has 5% - 0% lichen coverage. No vegetation is present. The terminus is lobate, steep and unstable, with a grade of approximately 72%. A low angle bench (5%

FTCm2 in Tamarack Canyon is a rock glacier deposit found at ~3680 m (Figure 14, pg. 50). Here FTCm2's terminal moraine is ~38 m high, composed of 80% fresh, angular,

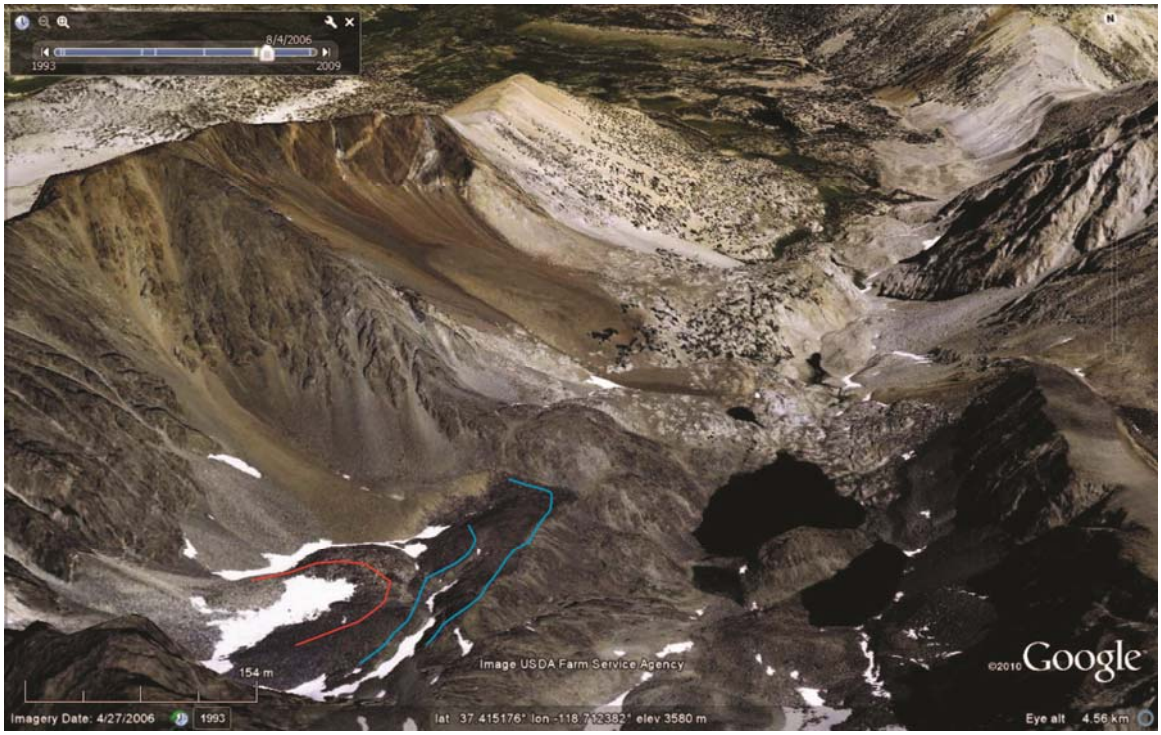

Figure 14: FTCm1 (blue) and FTCm2 (red) in Tamarack Canyon (image from Google Earth).

large boulders (1-3 m diameter) of basalt/diorite, and granodiorite (approximately 80%/20%), and has 5% - 0% lichen coverage. No vegetation is present. The terminus is lobate, steep and unstable, with a grade of approximately 72%. A low angle bench (5% slope) continues to the cirque headwall. FTCm2 on laps FTCm1 at the base of the terminus to the northeast.

In Francis Canyon FTCm1 is a rock glacier filling the canyon on the southeast side, is confined by FCm4 to the west, and extends from 3650 to 3430 m covering a map distance of 1,045 m. This rock glacier is onlapped by FTCm2 and has several lobate furrows 10 m in height and a slope of 215% showing flow direction to the northeast down canyon. It exhibits an average GWR of 67%. This advance was correlated to a similar deposit in Tamarack Canyon through similar GWRs, elevation, and stratigraphic

Figure 15: FTCm1 crosscutting FCm4.

relationships. There is little soil development and an increase to about 5% matrix with sections of up to about 10% to 15%. An increase in lichen cover can be seen from FTCm2, as well as an increase in granitic boulder oxidation. Clast composition is similar to FTCm2 with ~90% granodiorite and gabbro/diorite making the other ~10%. There is no woody vegetation.

FTCm1 in Tamarack has two lobate furrows ~8 m high indicating flow direction northeast. An average GWR of 48% fresh was obtained with a high of 50% and a low of 47%. There was a snowfield present at the back of the cirque. There was no interstitial ice, little soil development, and no vegetation. There is an increase in matrix from FTCm2 to about 5%. A slight increase in lichen cover on boulders can be observed from

FTCm2 to FTCm1. Boulder composition consists of ~60% gabbro/diorite and 40% granodiorite. FTCm1 is on lapped by FTCm2, making FTCm1 the older unit.

The next older deposit FCm4, marks the beginning of glacial deposits perched on the Plateau on the west side of Francis Canyon. FCm4 is cross cut by FTCm1 in the main canyon just to the east (Figure 15, pg. 51). This series of lobate moraines appear to be remnant moraines from a glacier that filled the canyon wall to wall, as evidenced by FCm4 forming an arc toward the main canyon. There is a perched moraine deposit at a similar elevation at the base of the east canyon wall that likely correlates with this unit. No data was collected from this deposit.

FCm4 terminates at a boundary characterized by an abrupt decrease of matrix and a significant increase in large (>1 m diameter) boulder frequency to the east, signifying the contact between the rock glacier (FTCm1) and the FCm4 moraine deposit. A similar contact is found near the west canyon wall between moraine and talus. The terminal section of this moraine faces northeast and overrides FCm3 and FCm2. This contact is recognized by a distinct lowering of slope and change in morainal form (Figure 7). FCm3 and FCm2 are both lateral moraines. FCm4 has an average of 36% fresh boulders and extends from 3558 to 3650 m and covers a map distance of 890 m. These moraines are more stable than FTCm2 and FTCm1 due to a significant amount of matrix (~45%) between boulders and decrease in slope. Furrows are approximately 15 m in height with a slope of ~50%. Sparse sage brush covers this unit.

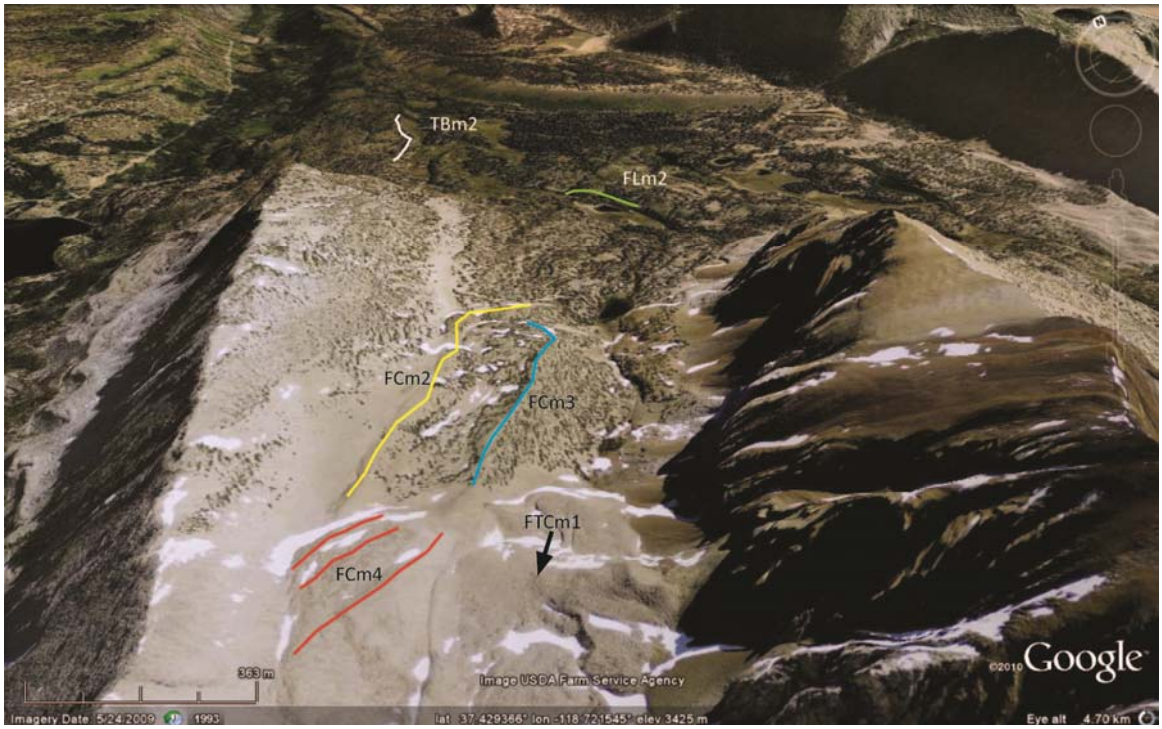

Figure 16: Unit crest locations (image from Google Earth).

Farther down canyon the moraine arcs southeast toward the main canyon, on laps FCm3, FCm2, and terminates under FTCm1. FCm3 and FCm2 are morphologically distinct because they extend out from under the arcuate moraines of FCm4 and continue linearly down canyon to the northeast (Figure 16, pg. 53). The moraine flank of FCm3 is less steep (~32% slope) than FCm4, with ~10% tree cover and an increase in matrix (~60%). FCm3 is a lateral moraine 23 m high with an average of 42% fresh boulders greater than 1 m in diameter. This moraine terminates at the edge of the Plateau in ~2 m high lobate furrows arcing toward the west canyon wall. These furrows are either the result of stranded ice or are a series of end moraines. There is slumping on the southeast and northeast flanks as well the occasional drainage incision of 1 m.

Figure 17: Samples DK-18 (left), DK-3 (right), DK-6 (bottom right).

FCm2 is stratigraphically older than FCm3, and it is an outer left lateral moraine with a height of 31 m, a slope of 36%, and an average of 27% fresh boulders. No distinction can be made between the vegetation cover of FCm3 and FCm2. There is an increase in matrix (~65%) between boulders. FCm3 and FCm2 both terminate indistinctly at the base of a ~37 m high Plateau into an area of sand just to the west of Francis Lake.

Terrestrial Cosmogenic Nuclide Dating

FCm3 had the highest elevation samples of sufficient quality to be considered. Samples were taken from its terminal moraine (Figure 3). The ages overlapped within 2σ

standard deviation of the internal uncertainty with one outlier (DK-19) at 16.1 ka (Figure 8). FCm3 yielded an average age of 13.7 ±1.9ka. Extremes of the sample population ranged from 16.1 ka to 11.3 ka. Best single sample was considered to be DK-18 at 12.6 ka ±0.5 with an external uncertainty of ±1.2 ka(Figure 17, pg. 54, left).

Samples from FLm2 (~3160 m) were taken from the outer right lateral near its terminus emerging from Francis Canyon (map, Plate 1). These ages place a lower limit on the last glacial advance to emerge from Francis Canyon. Three samples (DK-3, 4, 5) overlapped within 2σ standard deviation. Two outliers were DK-1, 2 at 11.7 ka and 13.2 ka respectively. The age spread ranged from 16.6 ka to 11.7 ka. The average age including outliers was 14.4 ±0.4 ka. The best single sample was DK-3 at 16.6 ±0.6 ka (Figure 17, right). This was the oldest sample with 2σ overlap. Out of the FLm2 samples it was the largest boulder and had the least self shielding.

TBm2 samples (~3100 m) were taken from the last terminal moraine on the Tamarack Bench (map, Plate 1). These dates represent a lower bounding age for the last full Tamarack Bench advance. Two outliers (DK-7, 10) based on 2σ internal uncertainty at 9 ka and 22.8 ka respectively. The remaining 3 samples (DK-6, 8, 9) overlapped. The complete age spread was constrained by the outliers at 9 ka to 22.8 ka. The average age was 16.8 ka ±0.5 ka. The best TBm2 sample was DK-6 at 18.6 ±0.5 ka with an external uncertainty of ±1.7 ka. DK-6 was the oldest in the 2σ cluster. Although not the largest boulder of TBm2, the surface had the lowest self shielding and had limited vegetation cover, minimizing fire spalling (Figure 17, bottom).

Relative Dating

Rinds

Average rinds of boulders generally support cosmogenic ages. However, a plot of rinds verse age for each individual sample revealed limited correlation (r^2=-.236) (Figure 18, pg. 57). TBm2 and FLm2 have the same average rind thickness of 6.2 mm. These are the oldest of the moraines sampled with average ages of 16.8 ka and 14.3 ka respectively. FCm3 has an average rind thickness of 7.4 mm and an average age of 13.7 ka. The oldest TBm2 sample (DK-10, 22.9 ka) has a rind thickness of 3 mm. DK-6 is the next oldest at 18.5 with a rind of 7 mm, the second thickest of TBm2. The thickest rind (DK-9) at 15 mm is the second youngest sample. DK-3 has the oldest age of FLm2 at 16.6 ka and the second thickest rind at 8 mm. DK-16 has the thickest rind of FLm2 at 12 mm but the youngest age with the largest uncertainty. From FCm3 samples DK-19 and 20 have the second largest rind at 8 mm and show the largest exposure ages from FCm3. DK-12 has the thickest second thickest rind of FCm4 (7 mm) with the oldest age of 12.2 ka.This sample had low current and a large uncertainty. DK-15 had the thinnest rind (4 mm) and the youngest age (17.7 ka) from FCm4.

Granite Weathering Ratios

TBm2 is stratigraphically the oldest morphological feature has the oldest average exposure age of 16.8 ka. The granite weathering ratio (GWR) of 44% suggests it has a

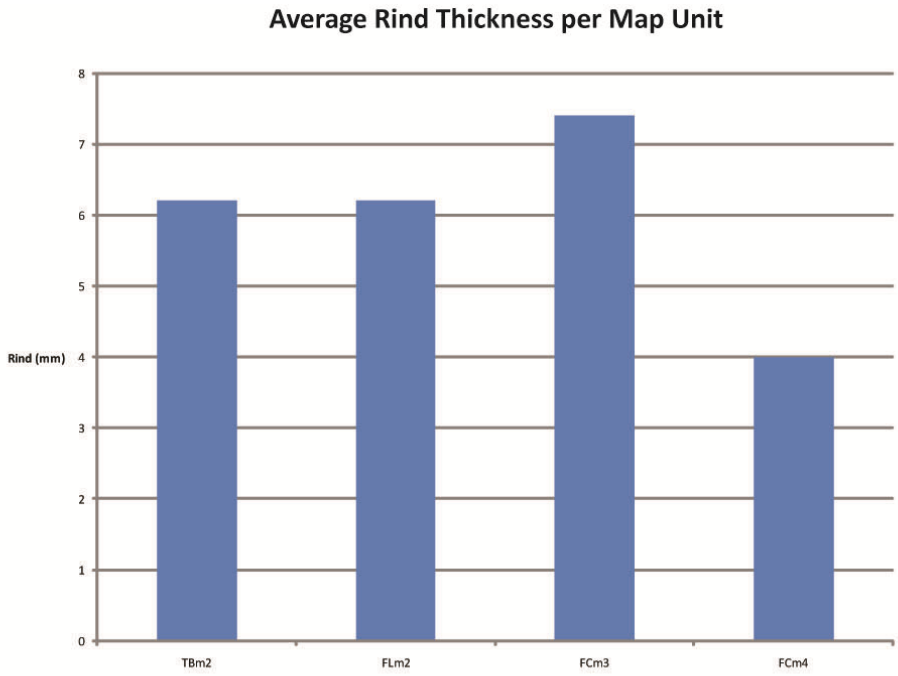

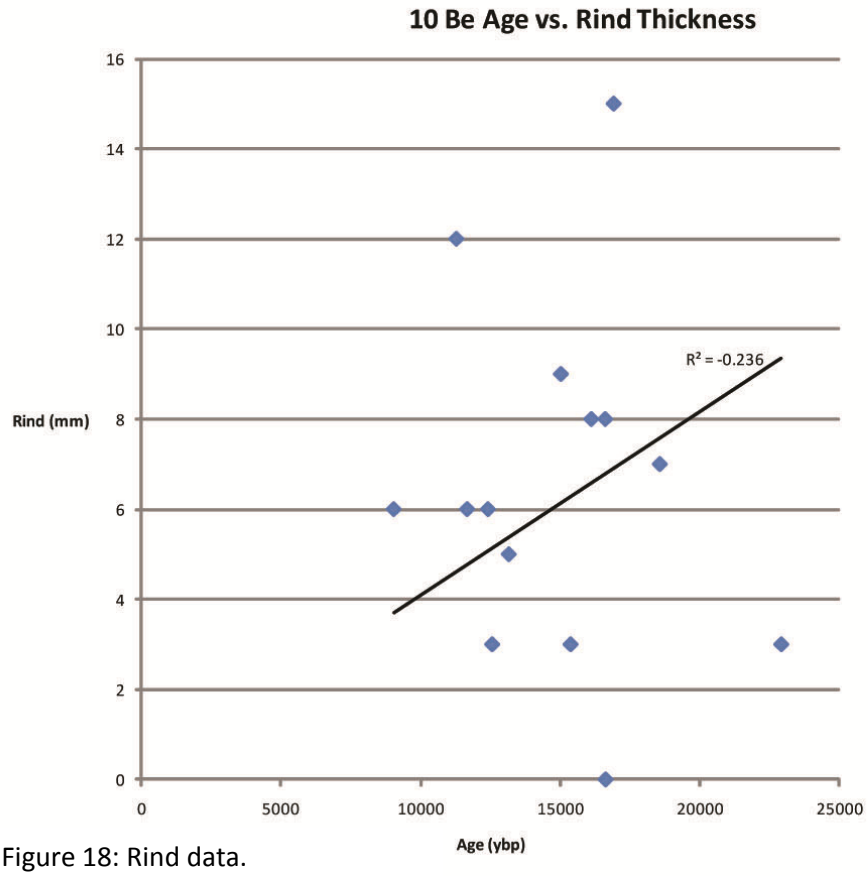

Figure 18: Rind data.

Figure 19: Relative Weathering Data
Francis Canyon/Tamarck Bench.

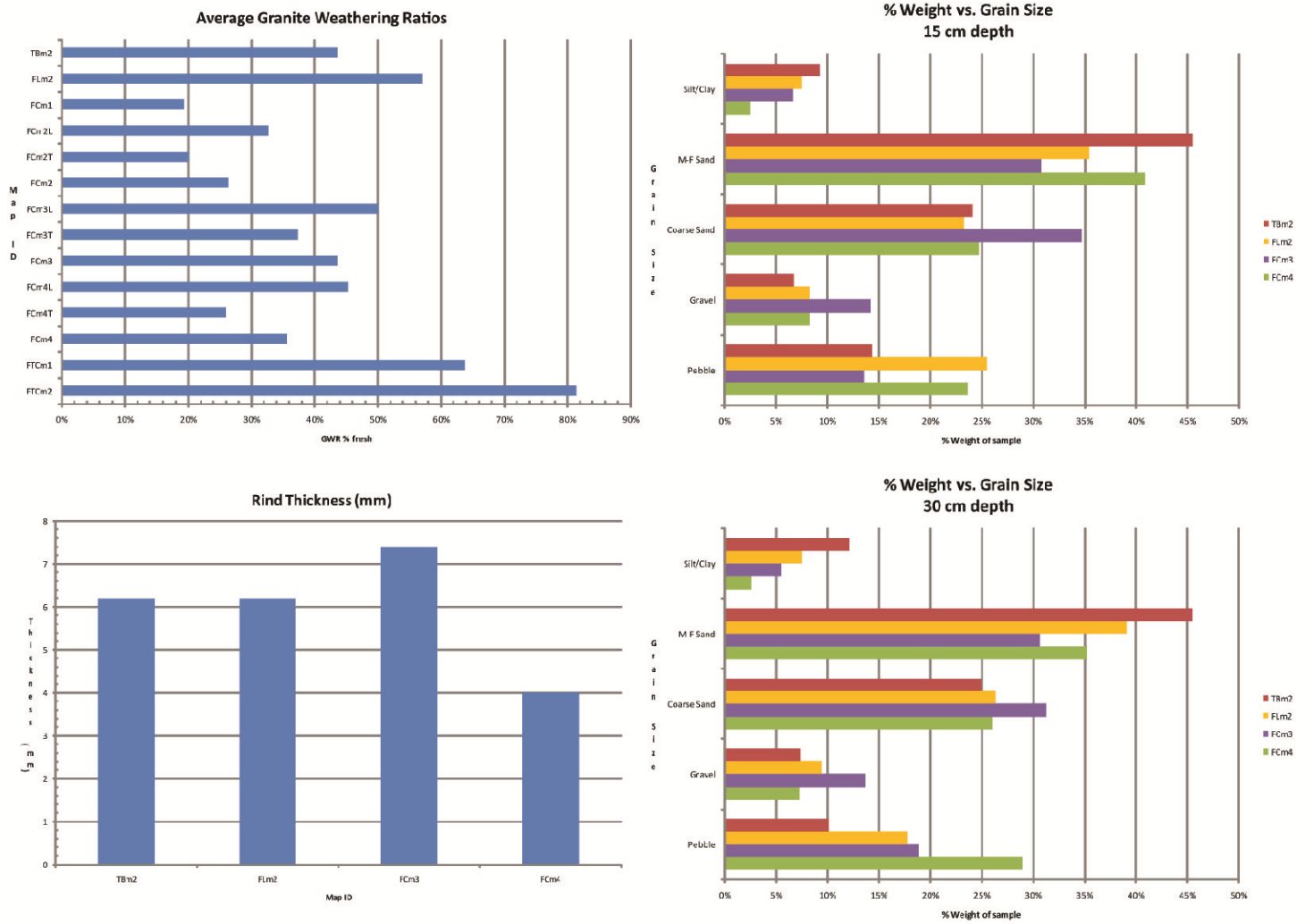

similar age relative to FCm3 (44%) (Figure 19, pg. 58). FLm2 has a GWR of 57% fresh, is the second oldest feature stratigraphically has the second oldest average exposure age (14.4 ka), and is the final feature confined to the bench.

In Francis Canyon, FCm1 has the lowest GWR of 19%, supporting its stratigraphic position. FCm2 has a GWR of 26% which supports its place in the Francis Canyon sequence. FCm3 has an average exposure age of 13.7 ka with a 44% GWR. The youngest feature sampled for exposure age (FCm4) has an average GWR of 36%. FTCm1 had a ratio of 64% and FTCm2 a ratio of 81%.

Soil

Average percent weight of silt/clay for both 15 and 30 cm depths correlated with TCN age. The oldest unit TBm2 has the highest average for 15/30 cm (9.2%, 7.4%). FLm2 has 7.5%/7.4% at 15 and 30 cm followed by FCm3 (6.7%, 5.5%) and FCm4 (2.5%, 2.5%). Pebble, gravel, and sand demonstrated no correlation to age.

Discussion

A standard method for assessing cosmogenic data is needed. Here I present a method of cosmogenic interpretation that combines current practices. Glacial transport (subglacial and supraglacial) brings boulders and debris to the moraine through a conveyer like motion. Subglacial debris is obtained through basal erosion and plucking. This debris falls from the slopes of the surrounding canyon walls and is entrained on the

surface of the glacier. Through the processes of rock fall and abrasion caused by glacial transport, the previously accumulated cosmogenic ^{10}Be is also removed (Owen *et al.*, 2002). Based on this theory, the measured ^{10}Be sampled from the surface of a boulder found on the crest of a moraine is the result of the exposure of that surface to the sky since deposition. This assumes that boulder has not been spalled due to fire and has not moved from that position by erosion since deposition. While the glacier advances or is stabilized, it is continuously depositing material at its terminus until retreat begins. Boulders located on the crest of the moraine are the last deposited before retreat due to the law of superposition. Therefore an ideal single TCN age is the length of time the surface of that particular boulder has been exposed to cosmogenic radiation. Inferred from this is length of time since deposition of the boulder, the length of time elapsed since final glacial deposition, and the age of the moraine. Based on the process of glacial deposition and inferences to be made, the following system is proposed for TCN interpretation. 1. Statistical elimination of outliers based on 2σ standard deviation of internal uncertainty. This will help identify surfaces that have pre-exposure inheritance and fire spalling. 2. Field conditions of boulder size, self shielding, snow cover, vegetation cover, location and proximity to canyon walls are used to confirm final identification of outliers. 3. Out of the remaining cluster of ages, the oldest age should be selected as the best representative sample for the geological feature. The oldest age should be the most accurate due to erosional effects on TCN accumulation. 4. After a

chronology is created within an area, external uncertainties (error associated with production rates) should be applied for correlation between studies.

Taking the average of boulder ages is problematic for the following reasons. A decision must be made to keep outliers or remove them. This will result in significantly different outcomes. The size of the internal uncertainties (AMS error) determines precision of the accepted cluster changing the significance of the average age. The effects of 1 and 2 do not allow for correlation between studies. It is important to report all TCN data collected: latitude, longitude, elevation, sample thickness, density, shielding correction, erosion rate, ^{10}Be atoms, ^{10}Be error with atoms, and the Be AMS standard so alternative interpretations and updated production rates can be applied allowing the study to remain relevant.

Intensity of spalling correlates with density of vegetation (Bierman and Gillespie, 1991). The moraine series on the Tamarack Bench and Francis canyon (TBm2, FLm2, and FCm3) are located in the subalpine (3000 – 3500 m) SN. Small amounts of litter accumulation and open stand structure of subalpine forests leads to infrequent fires (Fites-Kaufman *et al.*, 2007). Fire in the SN occurred on 200 year intervals in subalpine forests (Caprio and Lineback, 2002; Chang, 1996). Trees were absent or sparsely established in the subalpine central SN before 10 ka (Anderson, 1990). Therefore, the significance of fire spalling is reduced at high elevations in the SN, and young outliers in our data set are likely due to exhumation by erosion post deposition.

There should have been limited outliers in the data set according to Phillips *et al.* (2009) moraine erosion estimates and the previously mentioned fire history of SN subalpine forest. This suggests either a problem with the application of the statistical method, erosion estimates, or fire history estimates.

TCN Chronology

The above interpretation yields unit ages and internal uncertainties of: TBm2 (18.8 ±0.5 ka), FLm2 (16.6 ±0.6 ka), and FCm3 (12.6 ±0.5 ka). This scenario suggests a complex history after the LGM as evidenced by unit FLm1 between TBm2 and FLm2 (map, Plate 1) demonstrates a higher resolution record than is recorded in larger drainages. The differences in orientation, area, and distances (terminal moraine to closest end moraine) from FLm2 to FLm1 (.5 km), and FLm1 to TBm2 (.5 km) suggest they are individual re-advances. TBm2 encompasses the entire Tamarack Bench. FLm1 and FLm2 occupy only a small portion of the southwest side near the mouth of Francis Canyon (map, Plate 1). Differences in soil development and GWRs for TBm2 and FLm2 (9.2%, 7.5% silt/clay) (44%, 57%) support significant differences of exposure lengths in a semi-arid climate. GWRs for FLm2 (44%) and FCm3 (42%) are in contradiction to this succession. The percent silt/clay of FLm2 (7.5%) and FCm3 (6.7%) also suggest a significant passage of time between deposition of the units. The contradictions of GWRs between FLm2 and FCm3 and may be the result of differences in vegetation cover.

A different story develops if outliers are not removed. The chronology becomes: TBm2 (22.8 ±0.6 ka), FLm2 (16.6 ±0.6 ka), and FCm3 (16.1 ±0.4 ka). This succession shows FLm2 and FCm3 as coeval. The chronology based on averages with no outliers is as follows: TBm2 (16.8 ±0.4 ka), FLm2 (14.4 ±.4 ka), FCm3 (13.7 ±2 ka). The associated errors with the averages also allow FLm2 and FCm3 to be coeval. Soil data does not support these scenarios.

Unit FCm3's ambiguous position on the Plateau in Francis Canyon leaves its morphological identification uncertain. Its parallel orientation limits classification to lateral (left or right) or medial moraine. At its northeastern limit, FCm3 arcs toward the northwest and lowers in height to ~6 m. There is a mix of hummocky and discontinuous arcuate features inside this arc. This indicates multiple scenarios for classification. The hummocky and arcuate features could be the result of stranded ice cut off from a full canyon advance forming FCm3 in between the stranded ice and the main glacier as a left lateral/medial moraine. The arcuate features and FCm3 could also be the remains of a series of end moraines and a right lateral deposited by a glacier confined to the Plateau. A great difference in ice volume and climatic conditions are implied depending on the interpretation of FCm3 because the main glacier would have to fill the canyon to the level of the Plateau to deposit FCm3 as a left lateral moraine.

Regional and Global Correlations

External uncertainties need not be considered when creating a chronology within a study area, because all samples within a study area will be affected equally. But the correlation of TCN ages outside the study area, to different nuclides, regions, or to independent age records requires the use of the external uncertainty. External uncertainty is dominated by the error associated with production rates of TCNs. Currently uncertainty is in the range of ~10% for ^{10}Be, and 10-15% for ^{36}Cl (Dunai, 2010). Since the uncertainty in production rates translates directly into uncertainty of the exposure age, the ages cannot be known more accurately than the production rates (Dunai, 2010). This makes correlations to short lived climate events like the Younger Dryas (Wahrhaftig and Cox) problematic. The uncertainty (~10%) at 10 ka translates to ~±1 ka, the approximate duration of this event.

Regional and global correlation is important for resolving climate events between the Atlantic and Pacific Oceans. The Younger Dryas cooling event (12.9 - 11.7 ka) affected most of the Northern Hemisphere (Kaplan *et al.*, 2010). Greater spacial resolution must be obtained to completely understand the mechanisms behind this event. Western North American mountain range records are becoming more robust and are beginning to provide such resolution. Based on ^{14}C dates from lake cores the Younger Dryas can be found as far south in Western North America as Chilliwack Valley, British Columbia (11.5-11.2 ka cal yrs) (Saunders *et al.*, 1987). The YD in Snoqualmie Pass, Cascades and Mount Rainier, Cascades, the last Pleistocene advances are dated at

13-12.9, 13.3-12.8 ka cal yrs (Heine, 1998; Porter, 1976). These advances are correlative and support the current constraints on the Recess Peak advance of the SN, California. The YD is expressed in the Colorado Front Range as evidenced by a carbon date (12 ±.060 ka) from a lake core (Menounos and Reasoner, 1997).

The last Pleistocene advance in the SN is considered to be the Recess Peak. The current age constraint for its timing is 13.1 ±.09 ka (Clark and Gillespie, 1997) based on a ^{14}C date of organic silt at the gyttja/outwash transition from Baboon Lakes, Bishop Creek. This date is from a core of the inner most lake inside the inner most Recess Peak recessional moraine. A ^{14}C age from gyttja at the gyttja/outwash transition in the central Baboon Lake yielded an age of 12.8-12.7 ka (Clark and Gillespie, 1997). These ages are conflicting stratigraphically.

Four ^{36}Cl ages were obtained from the Recess Peak terminal moraine at Baboon Lakes yielding an average of 12.5 ±4.4 ka (10.4, 9.8, 11.2, 19.2 ka) (Phillips *et al.*, 2009), consistent with the age from the central Baboon Lake core. Based on field assessment, the best sample was considered to be the only sample from a terminal moraine in the South Fork of Bishop Creek at Treasure Lakes (13.3 ±0.6 ka) (Phillips *et al.*, 2009) and was considered representative of the advance. If the ~10-15% external uncertainty is considered, a possible Younger Dryas age cannot be ruled out.

A different conclusion is made if interpretation is performed using the sample selection method proposed in our study. If outliers are removed, the best representative sample becomes 11.2 ka because it is the oldest sample in the cluster. If

the external uncertainty of ~10%-15% is applied (±1.1-1.5 ka), this date agrees with the central Baboon Lake core of 12.8-12.7 ka, placing the advance within the time frame of the Younger Dryas interval (Kaplan *et al.*, 2010) as correlates with FLm2 from Francis Canyon of 12.6 ±1.2 ka (external uncertainty). However, these findings cannot unequivocally confirm or deny a Younger Dryas advance due to the stratigraphic contradiction of the Baboon Lake core ages and the error associated with TCN ages. Our best sample ages obtained from the Tamarack Bench, TBm2 (18.8 ±1.7 ka) and, FLm2 (16.6 ±1.6 ka) correspond with Phillips *et al.*'s (2009) Tioga 3 (18.5-17.0 ka) and Tioga 4 (16.0-14.5 ka).

Our TCN ages and external uncertainties are as follows with outliers included: TBm2 (22.8 ±2.1 ka), FLm2 (16.6 ±1.6 ka), and FCm3 (16.1 ±1.5 ka). This scenario makes FLm2 and FCm3 correlative within the internal uncertainties and places them at the LGM. TBm2 corresponds with (Phillips *et al.,* 1996; 2009) Tioga 2. If averages are used to represent the age of the moraine the chronology is: TBm2 (16.8 ±1.5 ka), FLm2 (14.4 ±1.3 ka), and FCm3 (13.7 ±2.3). The difference in these scenarios demonstrates the importance of having a standard method of interpretation for TCN data.

All moraines sampled generally correlate to MIS 2 (Figure 20, pg. 67). FCm3's best sample age of 12.5 ±1.2 ka correlates to a gradual warming of sea surface temperatures (SSTs) after returning to cooler conditions from a warm peak at ~17 ka as recorded in marine core ODP 1012 from Santa Barbara Basin (Herbert, 2001). FLm2 is centered on the initial cooling of SSTs in ODP 1012 and GISP 2 just before the Bolling

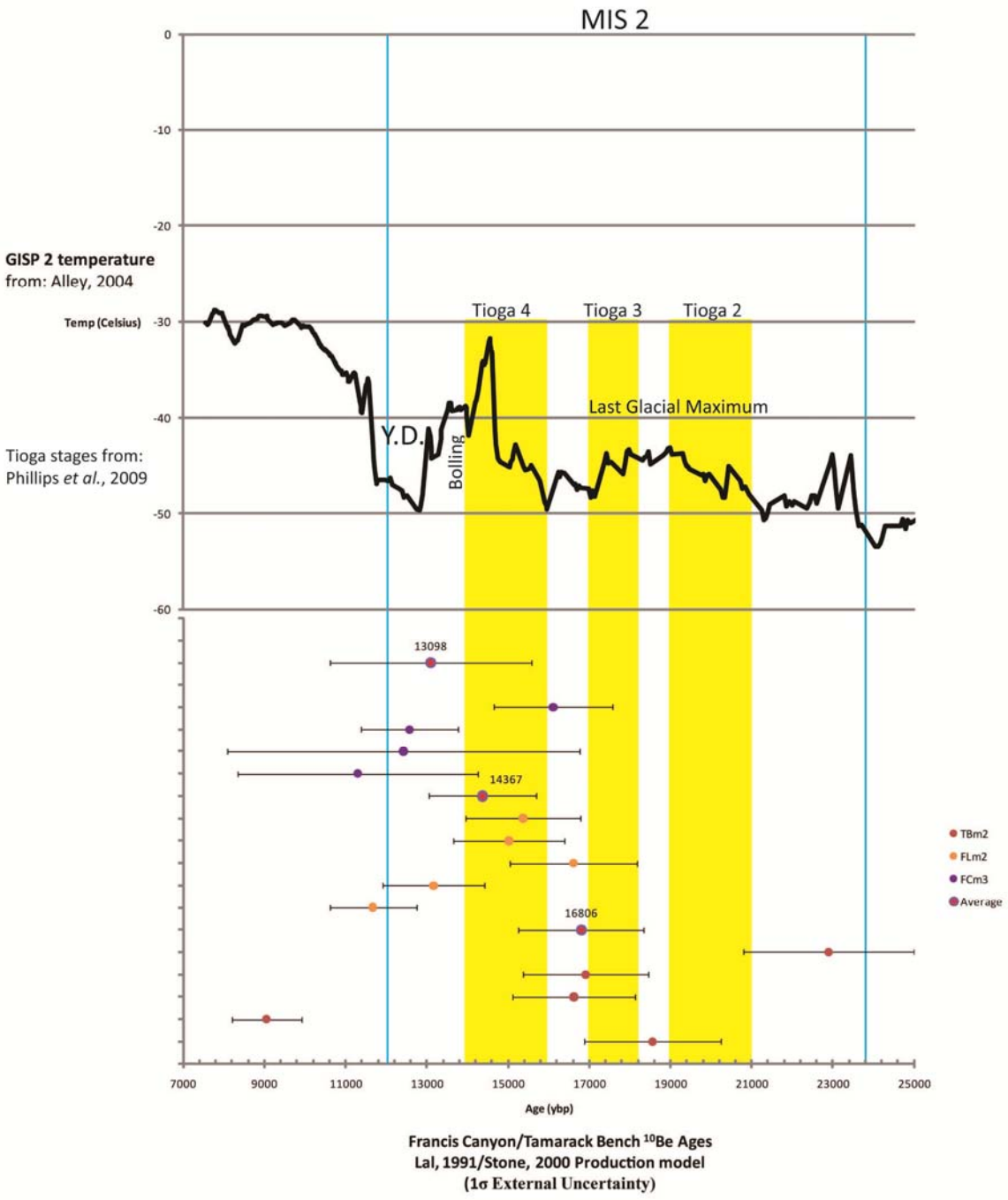

Figure 20: Francis Canyon and Tamarack Bench regional and global correlation.

warming event preceding Atlantic ice rafting event Heinrich 1 (H1) as seen in DSDP 609. TBm2 is approximately coeval with warming of SSTs in ODP 1012, cooling in ODP 893A (Hendy, 2007) and GISP II. Due to the large external uncertainties only approximations can be made.

Owen *et al*. (2003) TCN ^{10}Be ages of boulders from moraines on San Gorgonio in the San Bernadino Mountains of Southern California were recalculated using the newest production rate parameters as of the date of this writing. This recalculation significantly altered the ages (Figure 21, pg. 69; Table 8, pg. 70).

In the original study the age clusters were as follows: Stage IV (5-9 ka), Stage III (12-13 ka), Stage II (15-16 ka), and Stage I (18-20 ka) (Owen *et al*., 2003). Broad correlations to the Younger Dryas (Stage III), and GISP 2 LGM (Stages I and II) were suggested. These results show the region synchronous with global records. Recalculation split stage II into 2 clusters (Figure 21). The significant difference from the original study ages to the recalculated ages demonstrates a weakness in the method.

In TCN studies the most recent production rates should be used: Stage IV (10.8 ±1 ka), Stage III (15.8 ±1.4 ka), Stage II (2 groups) (18.6 ±1.7 ka and 42.2 ±3.9 ka), and Stage I (24 ±2.2 ka). Correlations made using the proposed interpretation method from our study are: Stage IV, FCm3, and Recess Peak; Stage III, FLm2, Tioga 4, Stadial 1 (S1) of OL 90/92 (Bischoff and Cummins, 2001); Stage II (group 1, largest cluster), TBm2, Tioga 3, S2; Stage IV, and S2.

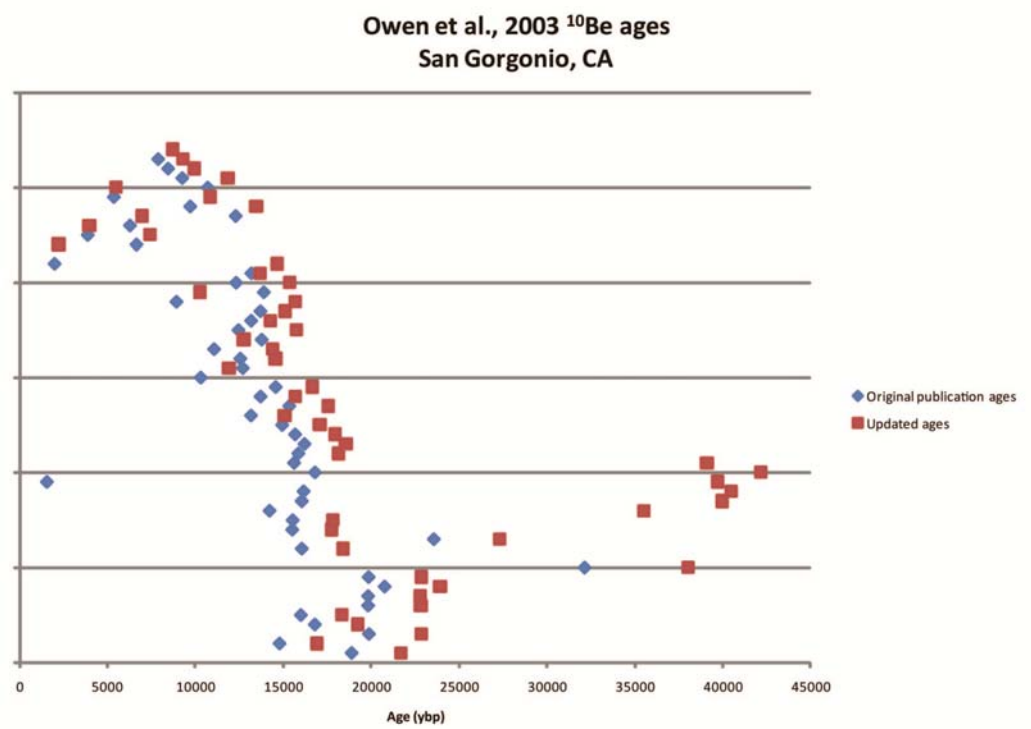

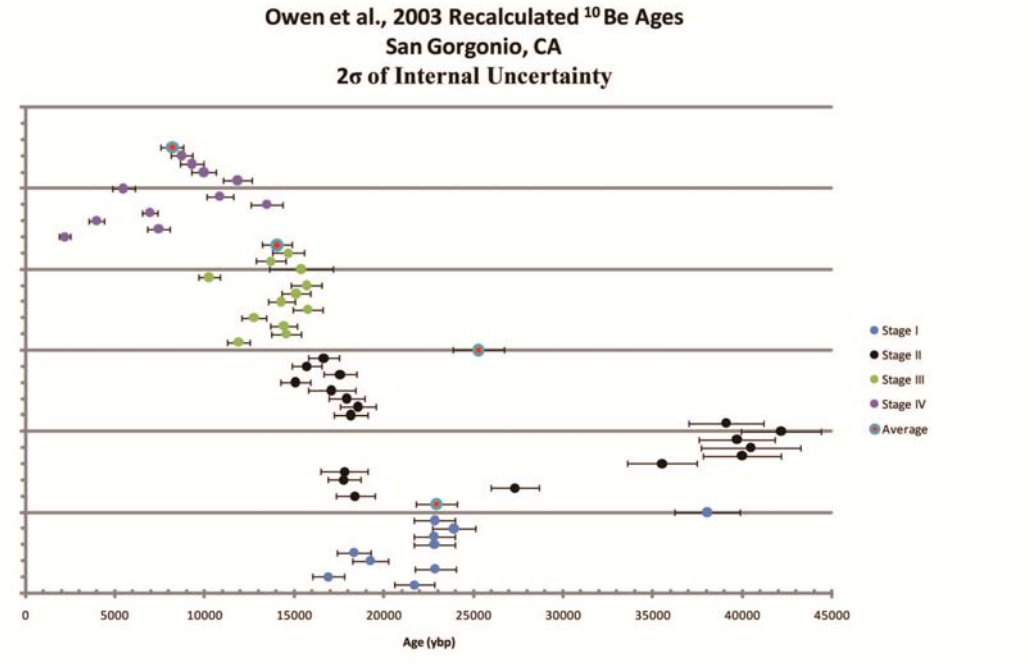

Figure 21: Owen *et al.,* 2003 recalculated data.

Table 8 Recalculated (Owen et al., 2003) San Gorgonio ^{10}Be study.

Results not dependent on spallogenic production rate model.					Time varying production models *met both best sample requirements.										
Owen et al., 2003			Lal (1991)/Stone (2000)			Desilets *et al.*		Dunai		Lifton *et al.*		Time-dependent	Best Sample (outliers)	Best Sample (No Outliers)
Stage I		Internal	External	2σ of Internal		(2003, 2006)	External	2001	External	2005	External	Lal (1991)/Stone (2000)	External	Previous
Sample ID	Age	Uncertainty	Uncertainty	Uncertainty	Sample ID	Age	Uncertainty	Age	Uncertainty	Age	Uncertainty	Age	Uncertainty	Publication Age
SG37	21711	547	1974	1094	SG37	20564	2492	20357	2456	19854	2029	20749	1834	18922
SG38	16912	439	1539	878	SG38	16250	1970	16180	1953	15736	1610	16368	1449	14822
SG39	22870	572	2078	1144	SG39	21585	2615	21347	2575	20839	2129	21788	1925	19909
SG40	19256	492	1751	984	SG40	18346	2223	18208	2197	17732	1813	18507	1637	16828
SG40b	18324	469	1666	938	SG40b	17508	2121	17397	2099	16936	1731	17655	1561	16033
SG20	22825	575	2075	1150	SG20	21523	2609	21288	2569	20778	2124	21748	1923	19860
SG25	22804	572	2073	1144	SG25	21727	2633	21471	2590	20994	2146	21741	1922	19861
SG26	23911	592	2172	1184	SG26	22693	2749	22406	2702	21931	2240	22715	2006	20800
SG27	22839	574	2076	1148	SG27	21766	2638	21507	2595	21031	2150	21773	1924	19890
SG28	38039	918	3460	1836	SG28	34556	4194	33835	4088	33270	3402	34738	3070	32174
Average	22940		2080		Average	21652	2624	21400	2582	20910	2137	21778	1925	19910
Stage II														
SG33	18396	545	1695	1090	SG33	17401	2124	17305	2103	16822	1738	17713	1589	16086
SG34	27320	671	2482	1342	SG34	25136	3046	24771	2988	24212	2473	25671	2267	23598
SG35	17771	454	1615	908	SG35	16852	2041	16774	2023	16300	1666	17144	1516	15545
SG36	17800	656	1686	1312	SG36	16875	2093	16797	2074	16322	1724	17170	1585	15568
SG1	35528	960	3258	1920	SG1	32303	3938	31659	3842	31093	3200	32636	2910	14254
SG2	39989	1079	3671	2158	SG2	35912	4381	35173	4272	34593	3563	36254	3235	16085
SG3	40482	1395	3816	2790	SG3	36279	4494	35540	4383	34966	3679	36626	3361	16190
SG4	39700	1046	3637	2092	SG4	35691	4349	34957	4240	34375	3535	36036	3208	1588
SG5	42163*	1119	3867	2238	SG5	37522	4575	36780	4465	36189	3725	37880	3376	16836
SG6	39095	1046	3585	2092	SG6	35280	4302	34547	4193	33975	3497	35567	3170	15645
SG7	18146	470	1652	940	SG7	17483	2119	17361	2095	16922	1731	17500	1549	15891
SG8	18557	511	1698	1022	SG8	17846	2170	17714	2145	17269	1774	17874	1591	16241
SG9	17932	490	1640	980	SG9	17288	2101	17173	2078	16737	1719	17305	1539	15707
SG10	17083	658	1629	1316	SG10	16497	2054	16411	2035	15981	1697	16529	1537	14973
SG21	15069	403	1374	806	SG21	14603	1772	14578	1761	14151	1450	14675	1302	13196
SG22	17554	458	1599	916	SG22	16894	2049	16797	2028	16358	1674	16957	1502	15375
SG23	15690	412	1429	824	SG23	15104	1831	15073	1820	14627	1497	15249	1351	13740
SG24	16654	420	1512	840	SG24	16086	1947	16015	1930	15583	1591	16137	1425	14602
Average	24280		2325		Average	23392	2855	23079	2804	22582	2330	23607	2112	15062
Stage III														
SG29	11906	317	1085	634	SG29	11333	1374	11380	1373	10982	1124	11592	1027	10343
SG30	14563	415	1336	830	SG30	13889	1690	13902	1685	13435	1383	14190	1267	12731
SG31	14412	373	1311	746	SG31	13739	1664	13756	1659	13292	1359	14048	1243	12590
SG32	12750	337	1161	674	SG32	12156	1473	12196	1472	11762	1204	12435	1102	11098
SG15	15766*	413	1436	826	SG15	15105	1831	15079	1820	14623	1496	15315	1357	13805
SG16	14284	378	1301	756	SG16	13752	1667	13758	1661	13314	1363	13931	1234	12486
SG17	15092	403	1376	806	SG17	14507	1760	14495	1751	14051	1439	14691	1303	13207
SG18	15685	430	1434	860	SG18	15056	1829	15030	1818	14577	1496	15242	1356	13734
SG19	10247	300	941	600	SG19	9828	1197	9888	1199	9551	984	9961	891	8960
SG48	15384	882	1606	1764	SG48	14746	1939	14730	1930	14277	1632	14964	1529	13926
SG49	13698	417	1265	834	SG49	13167	1608	13185	1604	12747	1319	13363	1201	12350
SG50	14667	450	1356	900	SG50	14089	1722	14090	1715	13638	1412	14291	1286	13218
Average	13881		1301		Average	13447	1646	13457	1641	13021	1351	13669	1233	12371
Stage IV														
SG11	2216	153	246	306	SG11	2369	324	2397	327	2343	282	2390	261	2027
SG12	7441	324	724	648	SG12	7021	884	7097	890	6880	742	7158	680	6685
SG13	3970	208	403	416	SG13	4231	546	4310	554	4188	468	4187	416	3912
SG14	6950	223	645	446	SG14	6628	811	6696	816	6511	676	6730	608	6314
SG45	13469	435	1252	870	SG45	12906	1582	12932	1579	12491	1299	13140	1189	12327
SG46	10850	369	1015	738	SG46	10362	1275	10418	1276	10058	1051	10552	961	9744
SG47	5468	318	572	636	SG47	5528	728	5581	732	5461	626	5522	566	5400
SG41	11849	405	1109	810	SG41	11304	1391	11349	1391	10957	1146	11536	1052	10734
SG42	9955	334	929	668	SG42	9476	1164	9548	1168	9194	959	9672	879	9289
SG43	9296	335	876	670	SG43	8801	1087	8877	1092	8549	899	8998	826	8484
SG44	8719	313	821	626	SG44	8225	1016	8300	1021	8007	841	8403	771	7920
Average	8198		781		Average	7896	983	7955	986	7694	817	8026	746	7531

An alternative interpretation that includes outliers is: Stage IV (13.5 ±1.3 ka), Stage III (15.8 ±1.4 ka), Stage II (42.2 ±3.9 ka), Stage I (38 ±3.5 ka). The resulting correlations using equivalent interpretations for our study data are: Stage IV, Recess Peak; Stage III, FCm3, FLm2, S1, Tioga 4; Stage I and Stage II coeval, and S2. This interpretation demonstrates the San Bernadino mountains and the SN as synchronous with the Cascades, but not with the Colorado Front range.

Stage II (15-16 ka), and Stage I (18-20 ka) showing synchroneity with GISP II. Regional correlations using equivalent interpretations are as follows: Stage III, FCm3, S1, Tioga 4; Stage II, FLm2, S1, Tioga 4; Stage I, TBm2, S1, Tioga 3.

In a regional lake core study in the SN Trumbower (2011) demonstrated synchroneity of Atlantic and Pacific climate systems throughout the Holocene. The Owens Lake record of rock flour proxy data shows general agreement with the Atlantic marine record (DSDP 609) and Greenland (GISP II) from 79- 15 ka (Bischoff and Cummins, 2001) (Figure 1). Open/closed regimes in Owens Lake occur in concert with GISP II from 155 to 60 ka, which also is in agreement with the Devils Hole record (Li *et al.*, 2004).

On the use of Relative Dating

Rind thicknesses showed poor correlation with TCN ages on an individual sample basis with a low R^2 value of 0.236. There was no discernable relationship between TCN age and rind thickness. FCm3's average rind thickness of 7.4 mm and average age of

13.7 ka was contradictory to age succession and stratigraphy (map, Plate 1). These results should be a warning to other researchers using rind thicknesses as a measure of relative age. The unexpected high GWRs of the two oldest units, TBm2 (44%) and FLm2 (57%), are due to the distinctly different nature of vegetation cover. Full size coniferous trees and sage brush cover on the Tamarack Bench likely contribute to more frequent/intense fires, and subsequent spalling comparative to the higher elevations of Francis Canyon moraines. The youngest feature sampled for exposure age (FCm4) has an average GWR of 36%. This supports its erroneous and anomalous average exposure age of 27.4 ka suggesting pre-exposure inheritance from rock fall. GWRs can assist in sample location selection and provide added insight to sample history.

Average weight of silt/clay from soil pits agrees with stratigraphy and TCN ages demonstrating it as a useful method of relative dating. However, the use of a single pit to represent a single moraine is not recommended based on end member values of the sample spreads, i.e. FLm2 (13.2%, 3.0%).

Conclusions

Based on the data collected and correlations made from the Francis Canyon/Tamarack Bench high altitude moraine series, the following conclusions were made. There is a need for a standard practice of TCN data interpretation. Differences in interpretation techniques lead to significantly different results. When comparing TCN studies with other nuclides, independent age constraints, or regional records, the

external uncertainty must be applied. The necessary data should be reported with each study so that up to date production rates can be applied for recalculation. It must be made certain the current production rates have been applied to the data in correlating TCN studies. This significantly alters the exposure ages. TCN ages cannot be used to conclusively resolve the timing of the millennial scale events (Wahrhaftig and Cox) due to large uncertainties associated with production rates of cosmogenic nuclides. More work needs to be done to conclusively constrain the Recess Peak advance in the SN. This will be resolved in time with the constantly increasing accuracy of TCN production rates.

The new data provided by this study presents a complex glacial history post LGM in the SN. FCm3's best sample age of 12.5 ±1.2 ka correlates to a gradual warming of sea surface temperatures (SSTs) after returning to cooler conditions from a warm peak at ~17 ka as recorded in marine core ODP 1012 from Santa Barbara Basin. FLm2 is centered on the initial cooling of SSTs in ODP 1012 and GISP II just before the Bolling warming event preceding Atlantic ice rafting event Heinrich 1 (H1) as seen in DSDP 609. TBm2 is approximately coeval with warming of SSTs in ODP 1012, cooling in ODP 893A and GISP 2.

Current data from the SN does not resolve the timing of the regional Recess Peak advance. Timing for Western North American alpine glacier advance across the Pleistocene/Holocene transition is crucial to understanding the mechanisms delivering moisture to the western United States.

References

1994b, Mt. Morgan Quadrangle, CA 7.5 Minute Series U.S. Geological Survey.

Anderson, R. S., 1990, Holocene Forest Development and Paleoclimates within the Central Sierra Nevada, California: Journal of Ecology, v. 78, p. 470-489.

Antevs, E., 1925, On the Pleistocene History of the Great Basin: Carnegie Institute of Washington: Quaternary Climates, v. 352, p. 51-114.

Antevs, E., 1938, Postpluvial Climatic Variations in the Southwest: American Meteorological Society Bulletin, v. 19, p. 190-193.

Balco, G., Stone, J., Lifton, N., and Dunai, T., 2008, A complete and easily accessible means of calculating surface exposure ages or erosion rates from 10Be and 26Al measurements: Quaternary Geochronology, v. 3, no. 3, p. 174-195.

Benson, L., Burdett, J., Lund, S., Kashgarian, M., and Mensing, S., 1997, Nearly synchronous climate change in the Northern Hemisphere during the last glacial termination: Nature, v. 388, p. 263-265.

Benson, L. V., Burdett, J. W., Kashgarian, M., Lund, S. P., Phillips, F. M., and Rye, R. O., 1996, Climatic and Hydrologic Oscillations in the Owens Lake Basin and Adjacent Sierra Nevada, California: Science, New Series, v. 274, no. 5288, p. 746-749.

Benson, L. V., May, H. M., Antweiler, R. C., and Brinton, T. I., 1998, Continuous Lake-Sediment Records of Glaciation in the Sierra Nevada Between 52,600 and 12,500 14C yr B.P.: Quaternary Research, v. 50, p. 113-127.

Bierman, P., and Gillespie, A., 1991, Range fires: a significant factor in exposure-age determination and geomorphic surface evolution: Geology, v. 19, p. 641-644.

Birkeland, P. W., Burke, R. M., and Walker, A. L., 1979, Soils and Subsurface Rock-Weathering Features of Sherwin and Pre-Sherwin Glacial Deposits, Eastern Sierra Nevada, California: Geological Society of America Bulletin, v. 91, p. 238-244.

Birman, J. H., 1964, Glacial Geology Across the Crest of the Sierra Nevada, California: GSA Special Papers, v. 75, p. 1-79.

Bischoff, J. L., and Cummins, K., 2001, Wisconsin glaciation of the Sierra Nevada (79,000–15,000 yr B.P.) as recorded by rock flour in sediments of Owens Lake, California: Journal of Quaternary Research, v. 55, p. 14-24.

Blackwelder, E., 1931, Pleistocene Glaciation in the Sierra Nevada and Basin Ranges: Bulletin of the Geological Society of America, v. 42, p. 865-922.

Burke, R. M., and Birkeland, P. W., 1979, Re-evaluation of Multiparameter Relative Dating Techniques and Their Application to the Glacial Sequence Along the Eastern Escarpment of the Sierra Nevada, California: Quaternary Research, v. 11, p. 21-51.

Caprio, A. C., and Lineback, P., Pre-twentieth centruy fire history of Sequoia and Kings Canyon National Parks: A Review and Evaluation of Our Knowledge., *in* Proceedings Proceedings of the Conference on Fire in California Ecosystems: Integrating Ecology, Prevention, and Management., San Diego, California, 2002, Volume Misc. Publication No. 1, Association for Fire Ecology p. 180-199.

Chang, C., 1996, Ecosystem Responses to Fire and Variations in Fire Regimes., *in* Center, W. R., ed., Sierra Nevada Ecosystem Project: Final report to Congress: Assessment and Scientific Basis for Management Options, Volume 11, Wildlands Resources Center, p. 1041-1070.

Clark, D. H., Bierman, P. R., and Larsen, P., 1995, Improving in Situ Cosmogenic Chronometers: Quaternary Research, v. 44, p. 367-377.

Clark, D. H., Clark, M. M., and Gillespie, A. R., 1994, Debris-Covered Glaciers in the Sierra Nevada, California, and Their Implications for Snowline Reconstructions: Quaternary Research, v. 41, p. 139-153.

Clark, D. H., and Gillespie, A. R., 1997, Timing and Significance of Late-Glacial and Holocene Cirque Glaciation in the Sierra Nevada, California: Quaternary International, v. 38/39, p. 21-38.

Curry, R. R., 1971, Glacial and Pleistocene History of the Mammoth Lakes Sierra, California:
A Geological Guidebook, Missoula, University of Montana Geology Dept.

Dalrymple, G. B., 1963, Potassium-argon ages of some Cenozoic volcanic rocks of the Sierra Nevada, California: Geological Society of America Bulletin, v. 74, p. 379-390.

Dorman, L. I., Valdes-Galicia, J. F., and Dorman, I. V., 1999, Numerical Simulation and Analytical Description of Solar Neutron Transport in the Earth's Atmosphere: Journal of Geophysical Research, v. 104, p. 22417-22426.

Dunai, T. J., 2010, Cosmogenic Nuclides: Principles, Concepts and Applications in the Earth Surface Sciences, Cambridge, Cambridge University Press, 187 p.:

Evans, D. J. A., 2005, Glacial Landsystems: London, Hodder Arnold, p. 373-387.

Finkel, R., and Suter, M., 1993, AMS in the Earth Sciences: Technique and Applications, Greenwich, JAI Press Inc., Advances in Analytical Geochemistry v. 1-114.

Fites-Kaufman, J., Rundel, P., Stephenson, N., and Weixelman, D. A., 2007, Montane and Subalpine Vegetation of the Sierra Nevada and Cascade Ranges, *in* Barbour, M., Keeler-Wolf, T., and Schoenherr, A. A., eds., Terrestrial Vegetation of California: Berkeley, University of California Press, p. 456-500.

Gillespie, A. R., and Zehfuss, P. H., 2004, Glaciations of the Sierra Nevada, California, USA: Quaternary Glaciations - Extent and Chronology Part II, p. 51-62.

Gosse, J. C., Klein, J., Evenson, E. B., Lawn, B., and Middleton, R., 1995, Beryllium-10 Dating of the Duration and Retreat of the Last Pinedale Glacial Sequence: Science, v. 268, p. 1329-1333.

Gosse, J. C., and Phillips, F. M., 2001, Terrestrial In Situ Cosmogenic Nuclides: Theory and Application: Quaternary Science, v. 20, p. 1475-1560.

Heine, J. T., 1998, Extent, Timing, and Climatic Implications of Glacier Advances Mount Rainier, Washington, USA, at the Pleistocene/Holocene Transition: Quaternary Science Reviews, v. 17, p. 1139-1148.

Hendy, I. L., 2007, Santa Barbara Basin ODP 893A Planktonic Foraminiferal Assemblage Data, *in* Paleoclimatology, I. P. W. D. C. f., ed.: Boulder, NOAA/DCDC Paleoclimatology Program.

Henry, C. D., 2009, Uplift of the Sierra Nevada, California: Geology, v. 37, no. 6, p. 575-576.

Herbert, T. D., 2001, Collapse of the California Current During Glacial Maxima Linked to Climate Change on Land: Science, v. 293, no. 5527, p. 71-76.

Huber, N. K., 1981, Amount and timing of Cenozoic uplift and tilt of the central Sierra Nevada, California - Evidence from the upper San Joaquin River: U.S. Geological Survey Professional Paper, v. 1197, p. 28.

Kaplan, M. R., Schaefer, J. M., Denton, G. H., Barrell, D. J. A., Chinn, T. J. H., Putnam, A. E., Andersen, B. G., Finkel, R. C., Schwartz, R., and Doughty, A. M., 2010, Glacier retreat in New Zealand during the Younger Dryas stadial: Nature, v. 467, p. 194-197.

King, B. L., 2010, The Post-Last Glacial Maximum Glacier Record of the Tamarack Bench, Eastern Sierra Nevada, California [Master of Science: University of California.

Konrad, S. K., and Clark, D. H., 1998, Evidence for an Early Neoglacial Glacier Advance from Rock Glaciers and Lake Sediments in the Sierra Nevada, California, USA: Arctic and Alpine Research, v. 30, no. 3, p. 272-284.

Lal, D., and Peters, B., 1967, Handbook of Physics, Berlin, Springer, Cosmic Ray Produced Radioactivity on Earth.

Li, H.-C., Bischoff, J. L., Ku, T.-L., and Zhu, Z.-Y., 2004, Climate and Hydrology of the Last INterglaciation (MIS 5) in Owens Basin, California: Isotopic and Geochemical Evidence from Core OL-92: Quaternary Science Reviews, v. 23, p. 49-63.

Masarik, J., and Beer, J., 1999, Simulation of Particle Fluxes and Cosmogenic Nuclide Production in the Earth's Atmosphere: Journal of Geophysical Research, v. 104D, p. 12099-12111.

Menounos, B., and Reasoner, M. A., 1997, Evidence for Cirque Glaciation in the Colorado Front Range during the Younger Dryas Chronozone: Quaternary Research, v. 48, p. 38-47.

Minnich, R. A., 2007, California climate and paleovegitation, *in* Barbour, M. G., Keeler-Wolf, T., and Schoenherr, A. A., eds., Terrestrial Vegitation of California, University of California press, p. 43-70.

Nishiizumi, K., Kohl, C. P., Arnold, J. R., Winterer, E. L., Lal, D., Klein, J., and Middleton, R., 1989, Cosmic Ray Production rates of 10Be and 26 Al in Quartz from Glacially Polished Rocks: Journal of Geophysical Research, v. 94, no. B12, p. 17907-17915.

Owen, L. A., Finkel, R. C., Caffee, M. W., and Gualtieri, L., 2002, Timing of Multiple Late Quaternary Glaciations in the Hunza Valley, Karakoram Mountains, Northern Pakistan: Defined by Cosmogenic Radionuclide Dating of Moraines: Geological Society of America Bulletin, v. 114, no. 5, p. 593-604.

Owen, L. A., Finkel, R. C., Minnich, R. A., and Perez, A. E., 2003, Extreme southwestern margin of late Quaternary glaciation in North America: Timing and controls: Geology, v. 31, p. 729-732.

Owen, L. A., Gualtieri, L., Finkel, R. C., Caffee, M. W., Benn, D. I., and Sharma, M. C., 2001, Cosmogenic Radionuclide Dating of Glacial Landforms in the Lahul Himalaya, northern India: Defining the Timing of Late Quaternary Glaciation: Journal of Quaternary Science, v. 16, p. 555-563.

Phillips, F. M., Stone, W. D., and Fabryka-Martin, J. T., 2001, An Improved Approach to Calculating Low-energy Cosmic-ray Neutron Fluxes at the Land/Atmosphere Interface: Chemical Geology, v. 175, p. 689-701.

Phillips, F. M., Zreda, M., Plummer, M. A., Elmore, D., and Clark, D. H., 2009, Glacial geology and chronology of Bishop Creek and vicinity, eastern Sierra Nevada, California: GSA Bulletin, v. 121, p. 1013-1033.

Phillips, F. M., Zreda, M. G., Benson, L. V., Plummer, M. A., Elmore, D., and Sharma, P., 1996, Chronology for Fluctuations in Late Pleistocene Sierra Nevada Glaciers and Lakes: Science, v. 274, no. 5288, p. 749-751.

Phillips, F. M., Zreda, M. G., Smith, S. S., Elmore, D., Kubik, P. W., and Sharma, P., 1990, Cosmogenic Chlorine-36 Chronology for Glacial Deposits at Bloody Canyon, Eastern Sierra Nevada: Science, v. 248, no. 4962, p. 1529-1532.

Porter, S. C., 1976, Pleistocene Glaciation in the Southern Part of the North Cascade Range, Washington: Geological Society of America Bulletin, v. 87, p. 61-75.

Porter, S. C., and Swanson, T. W., 2008, 36Cl dating of the classic Pleistocene glacial record in the northeastern Cascade Range, Washington: American Journal of Science, v. 308, no. 2, p. 130-166.

Powell, D., and Klieforth, J., 2000, Weather and Climate, Sierra East: Edge of the Great Basin: Los Angeles, University of California Press, p. 70-93.

Reimer, P. J., Baillie, M. G., Bard, E., Bayliss, A., Beck, J. W., Blackwell, P. G., Bronk Ramsey, C., Buck, C. E., Burr, G. S., Edwards, R. L., Friedrich, M., Grootes, P. M., Guilderson, T. P., Hajdas, I., Heaton, T. J., Hogg, A. G., Hughen, K. A., Kaiser, K. F., Kromer, B., McCormac, F. G., Manning, S. W., Reimer, R. W., Richards, D. A., Southon, J. R., Talmo, S., Turney, C. S., Van der Plicht, J., and Weyhenmeyer, C. E., 2009, IntCal09 and Marine09 radiocarbon age calibration curves, 0-50,000 years cal BP: Radiocarbon, v. 51, p. 1111-1150.

Russell, I. C., 1885, Existing Glaciers of the United States: Fifth Annual Report of the United States Geological Survey, *in* Survey, U. S. G., ed.: Washington, Washington Government Printing Office, p. 1-355.

Saunders, I. R., Clague, J. J., and Roberts, M. C., 1987, Deglaciation of Chilliwack River Valley, British Columbia: Canadian Journal of Earth Sciences, v. 24, p. 915-923.

Sharp, R. P., 1969a, Semiquantitative Differentiation of Glacial Moraines Near Convict Lake, Sierra Nevada, California: The Journal of Geology, v. 77, p. 68-91.

Sharp, R. P., 1969b, Semiquantitative Differentiation of Glacial Moraines Near Convict Lake, Sierra Nevada, California: Journal of Geology, v. 77, p. 68-91.

Sharp, R. P., and Birman, J. H., 1963, Additions to Classical Sequence of Pleistocene Glaciations, Sierra Nevada, California: Geological Society of America Bulletin, v. 74, p. 1079-1086.

Synal, H.-A., 1995, Accelerator Mass Spectrometry: New Applications: Applied Radiative Isotopes, v. 46, no. 6/7, p. 457-466.

Trumbower, M., 2011, Regional Trends in Holocene Glaciation of the Southeastern Sierra Nevada, California. [Master of Science: University of California.

USDA, 2008, Inyo National Forest Atlas U.S. Geological Survey.

Wahrhaftig, C., and Cox, A., 1959, Rock Glaciers in the Alaska Range: Geological Society of America Bulletin, v. 70, no. 4, p. 383.

Zreda, M. G., and Phillips, F. M., 1994, Cosmogenic 36 Cl Accumulation in Unstable Landforms 2. Simulations and Measurements on Eroding Moraines: Water Resources Research, v. 30, p. 3127-3136.

GLACIAL DEPOSITS OF EASTERN ROCK CREEK AND LOWER ROCK CREEK CANYON

Plate 1

Explanation for unit distinctions

Glacial deposits and features

FTCm2

Lobate moraines ~40 m high, ~77% slope, located in Francis and Tamarack Canyons at 3680 m elevation. Composed of ~1-3 m diameter boulders, (~73-87% fresh), 0-5% matrix, no vegetation. Onlaps FTCm2.

FTCm1

Lobate moraines and furrows with ~10 m relief, 215% slope, located in Francis and Tamarack Canyons extending between 3430-3563 m elevation. Moraine crests composed of boulders ranging from ~0.25-2 m diameter (~77% fresh) boulders, ~5% matrix with sections of ~10-15%, no vegetation. Moraines onlapped by FTCm1.

FCm4

Series of lobate moraines unique to Francis Canyon ~15 m high, ~50% slope, and extend from 3540-3610 m elevation. Moraine crests composed of boulders ~0.25-2 m diameter (44% fresh), ~45% matrix, and ~1% brush cover. Onlaps FCm2 and FCm3 to the northeast, and is cross cut by FTCm2 where frontal lobes arc to the east.

FCm3

Lateral moraine trending northeast, ~23 m high, with ~32% slope, extending between ~3400-3535 m elevation. Moraine crest is composed of boulders ~0.25-2 m diameter, 54% fresh boulders, 60% matrix fill, with ~10% 0.1-1 m tall low lying trees. Moraine is onlapped by FCm1 to the southwest.

FCm2

Lateral moraine parallel to FCm2 trending northeast, ~31 m high, 36% slope, between 3400-3535 m elevation. Moraine is composed of boulders ~0.25-2 m diameter (~27% fresh), 10% 0.1-1 m tall low lying trees. FCm1 cross cuts it to the southwest.

FCm1

Lateral moraine trending northwest to southeast at ~3330 m elevation. ~20 m high. Extends out from TBm2 for ~300 m.

FLm2

Concentric terminal moraines face southeast toward Francis Lake canyon on the southwest of the Tamarack Bench. Well-preserved moraines ~4-10 m high dam Kenneth Lake. Truncate FLm1 moraines. Composed of ~57% fresh boulders. Lowest terminal moraine at ~3150 m elevation.

FLm1

Concentric terminal moraines face south to southeast toward Francis Lake canyon on the southwest of the Tamarack Bench. Well-preserved moraines between ~5-10 m high. Truncate TBm2 deposits to the west and are truncated by FLm2 moraines to the south. Lowest terminal moraine at ~3110 m elevation. Composed of ~29% fresh boulders.

TLm2

Concentric terminal moraines face south up the Tamarack Lakes canyon in the southeast of the Tamarack Bench. Truncates TLm1 lateral moraines to the east and are truncated by Ma. Moraines ~20 m high dam two lakes. Composed of ~64% fresh boulders. Lowest terminal moraine at ~3195 m elevation.

TLm1

Concentric terminal moraines face southeast in the east and northeast of the Tamarack Bench. Moraines are truncated by TLm2 moraines to the southeast. Well-preserved morphology dams multiple lakes. Moraines ~5-10 m high. Composed of ~49% fresh boulders. Lowest terminal moraine at ~3172 m elevation.

TBm2

Terminal moraines truncate TBm1 lateral moraines on the Tamarack Bench. Lateral moraines onlap RCm1 lateral moraines and are truncated by FLm1 moraines to the west. Moraines range from ~6-16 m high. Streams have incised ~10 m since deposition. Deposits composed of ~32% fresh boulders. Lowest terminal moraines at ~3095 m elevation.

TBm1

Moraines on the Tamarack Bench which are concentric to the southeast and confined laterally by TBm1 deposits, and are truncated by TBm2 terminal moraines updrainage. Terminal moraines ~8 m high. Streams have incised ~5-8 m. Comprised of ~27% fresh boulders. Lowest terminal moraine at ~3085 m elevation.

RCm3

Terminal moraines face concentrically to the east. Terminal moraines ~7 m high and display wellpreserved morphology. Lateral moraines ~3m high. Contain ~10% fresh boulders. Soil is well-developed and vegetated with large trees. Lowest terminal moraine at ~2965 m elevation first mapped by Birman (1964) as Recess Peak.

RCm2

Moraines confined to Rock Creek. Lateral moraines ~150 m high in Rock Creek. Terminal moraines highly eroded but morphology is mostly preserved. Contain ~18% fresh boulders. Lowest terminal moraine at ~2860 m elevation first mapped by Birman (1964) as Hilgard.

RCm1

~15-30 m high lateral moraines on the Tamarack Bench and ~180 m high in Rock Creek. Terminal moraine in Rock Rock Creek highly altered by drainage development. Contain ~10% fresh boulders. Lowest terminal moraine at ~2712 m elevation first mapped by Birman (1964) as Tioga.

PRCm1

Glacial deposits older than RCm1. Include lateral moraines ~180 m high on the Tamarack Bench and ~260 in Rock Creek. Moraine crest's traceable ~10 km downstream to the Sherwin grade. Lowest terminal moraine at 2282 m elevation.

Ut

Undifferentiated till and ground moraines. No distinct correlative relationships exist between this till and other glacial deposits.

RM

Roche Moutonee. Outcrop of bedrock streamlined in direction of ice flow.

RGvw

Valley wall rock glacier deposit, composed of ~45% fresh boulders, ~0 - 5% matrix, boulders ~1 - 3 m in diameter, multiple lobes and furrows ~3 m high, found from 3300 - 3160, no distinct correlation between deposits

Gbr

Bedrock exhibiting evidence of glaciation; striations, polish and/or erratics.

Geologic features

Br — *Exposed bedrock*

Ls — *Deposits of gravity flow or mass wasting*

Tal — *Colluvium deposits*

Flu — *Fluvial and glaciofluvial deposits*

Other

Moraine Crests

Streams

Lakes

Glacier

Certain contact

Approximate contact

SCALE 1:16,000

1 0.5 0 Kilometers 1 2

1,000 500 0 Meters 1,000 2,000

CONTOUR INTERVAL 40 FEET

N

Glacial geology collected and compiled by Kennedy, M.J., King, B.L., Kohut, D.L. and Trumbower, M.W.